ANL-ART-168

Initial Development of an Improved Creep-Fatigue Design Method that Avoids the Separate Evaluation of Creep and Fatigue Damage and Eliminates the Requirement for Stress Classification

Applied Materials Division

ANL-ART-168

Initial Development of an Improved Creep-Fatigue Design Method that Avoids the Separate Evaluation of Creep and Fatigue Damage and Eliminates the Requirement for Stress Classification

---

Applied Materials Division
Argonne National Laboratory

August 2019

Prepared by

M. C. Messner, Argonne National Laboratory
Robert I. Jetter, R. I. Jetter Consulting
Yanli Wang, Oak Ridge National Laboratory
T.-L. Sham, Argonne National Laboratory

Abstract

This report describes a method for capturing the effect of strain range, temperature, hold time, and elastic follow up on the cyclic life of a material undergoing uniaxial load. Developing design correlations of this type requires methods for extrapolating experimental data as a function of hold time and follow up factor. Various extrapolation methods are developed and discussed here and recommendations are developed for the final approaches to be adopted for design use. The report also describes comparisons between the new creep-fatigue design method, described here, and current creep-fatigue design methods in the ASME Boiler and Pressure Vessel Code and associated nuclear Code Cases. These comparisons demonstrate several advantages of the new method: it is easier to execute and is less over conservative than many current approaches. This report, along with a companion on extending these results to multiaxial load and on combining load cycles, represents the accumulation of several years of work on the development of this new approach to creep-fatigue design, combining an elastic perfectly plastic analysis method with simplified model tests measuring the effect of elastic follow up on creep-fatigue cyclic life. The conclusions to this report describe a path forward to developing the required design data for high temperature advanced reactor structural materials and guiding the adoption of the new method in the ASME Boiler and Pressure Vessel Code and related standards.

Table of Contents

Abstract i
Table of Contents iii
List of Figures v
List of Tables vii
1 Introduction 1
1.1 Overview . . . 1
1.2 Elastic follow up . . . 2
2 Extrapolating data from SMT tests 5
2.1 Deformation . . . 5
2.2 Damage . . . 9
2.2.1 Methods using creep-fatigue interaction . . . 9
2.2.2 A unified method: dissipated work . . . 13
3 Preliminary design curves 17
3.1 Scaling directly from experimental data . . . 17
3.2 Constructing design curves from Code data . . . 21
3.2.1 Time fraction . . . 21
3.2.2 Work-based . . . 24
3.2.3 Coffin-shift to design fatigue curves . . . 34
4 Creep-fatigue design method for uniaxial loading 39
4.1 Additional design curves . . . 39
4.2 Uniaxial design method . . . 39
4.3 Comparison to current ASME methods . . . 45
5 Conclusions 51
A Alloy 617 test database 53
Acknowledgments 57
Bibliography 59

List of Figures

1.1 Schematic illustration of the effect of elastic follow up on the (a) stress/strain behavior and (b) stress/time behavior of an elastic-creep material undergoing stress relaxation. . . . 3

2.1 Schematic of the simple two bar model used to derive extrapolation formula for uniaxial creep-fatigue loading with follow up. . . . 6
2.2 Example cyclic stress-strain curve. Notional results from a strain-controlled cyclic fatigue test with increasing strain range are plotted in blue. The resulting cyclic stress-strain curve is plotted in black. . . . 8
2.3 Notional creep-fatigue interaction diagrams illustrating the difference between a linear and a bilinear interaction. . . . 10
2.4 Schematic showing the partitioning of dissipated energy into fatigue (W_{base}), creep-fatigue (W_{hold}), and follow up (W_q) contributions. . . . 14

3.1 Design curve fit to experimental Alloy 617 data at 950° C using the base Coffin model (Eq. 3.2). . . . 19
3.2 Design curve fit to experimental Alloy 617 data at 950° C using the modified Coffin model (Eq. 3.3). The red and green lines overlap. . . . 20
3.3 The modified Coffin model (Eq. 3.3) with the parameters given in Table 3.2 compared to the full Alloy 617 dataset for $q = 1$, including the small strain range data. The red and green lines overlap. . . . 21
3.4 Design curve constructed by shifting the nominal ASME fatigue curve by the Coffin-shift predicted by (Eq. 3.3). The red and green lines overlap. . . . 22
3.5 EPP+SMT design curves for Alloy 617 at 950° C constructed with nominal material properties using the time-fraction approach and the ASME database compared to the experimental data. . . . 23
3.6 Design curves constructed with the time-fraction approach from the ASME design data for Alloy 617 at $T = 500°$ C. . . . 25
3.7 Design curves constructed with the time-fraction approach from the ASME design data for Alloy 617 at $T = 700°$ C. . . . 26
3.8 Design curves constructed with the time-fraction approach from the ASME design data for Alloy 617 at $T = 900°$ C. The 10,000 hour hold curve is off the plot, the material cannot survive even a single cycle with that length of hold. . . . 27
3.9 Design curves constructed with the time-fraction approach from the ASME design data for 316H at $T = 500°$ C. . . . 28
3.10 Design curves constructed with the time-fraction approach from the ASME design data for 316H at $T = 575°$ C. . . . 29
3.11 Design curves constructed with the time-fraction approach from the ASME design data for 316H at $T = 650°$ C. . . . 30
3.12 Correlation between work-per-cycle (W_{avg}) and cycles to failure (N) for the 850° C Alloy 617 data. . . . 32
3.13 Correlation between work-per-cycle (W_{avg}) and cycles to failure (N) for the 950° C Alloy 617 data. . . . 32

3.14 Correlation between corrected work-per-cycle (W_{corr}) and cycles to failure (N) for the 850° C Alloy 617 data. 33
3.15 Correlation between corrected work-per-cycle (W_{corr}) and cycles to failure (N) for the 950° C Alloy 617 data. 34
3.16 EPP+SMT design curves for Alloy 617 at 950° C constructed with nominal material properties using work-based approach compared to the experimental data. 35
3.17 Design curves constructed with the standard Coffin shift starting from the Alloy 617 design fatigue curves at $T = 950°$ C. 36
3.18 Design curves constructed with the saturating, modified Coffin shift starting from the Alloy 617 design fatigue curves at $T = 950°$ C. 37

4.1 (a) Coffin and (b) modified Coffin shifts fit to the experimental Grade 91 fatigue and creep-fatigue data at 538° C. 40
4.2 (a) Coffin and (b) modified Coffin shifts fit to the experimental Grade 91 fatigue and creep-fatigue data at 593° C. 40
4.3 Prospective design curves for Grade 91 using the standard Coffin shift at 538° C. 41
4.4 Prospective design curves for Grade 91 using the modified Coffin shift at 538° C. 42
4.5 Prospective design curves for Grade 91 using the standard Coffin shift at 593° C. 43
4.6 Prospective design curves for Grade 91 using the modified Coffin shift at 593° C. 44
4.7 Schematic illustrating the effect of a constant shift on a log scale to a fatigue curve in the low cycle and high cycle regimes. As the material approaches the fatigue limit a shift has no effect on the design curve. 48

5.1 Sketch demonstrating two reasonable approaches to extrapolating the available high strain range, short hold time experimental data into the low strain range, long hold regime needed for engineering design. 52

List of Tables

3.1 Parameters for the base Coffin model (Eq. 3.2). 18
3.2 Parameters for the modified Coffin model (Eq. 3.3). 18
3.3 Optimal values of C for the corrected work predictor. 33

4.1 Parameters used in the sample design problem. 46
4.2 Results from the comparative analysis of the two bar system accounting for the creep-fatigue design checks only. Hold time is 100 hours. Methodologies are design by *E*lastic analysis, design by *E*lastic *P*erfectly-*P*lastic analysis, design by *I*nelastic analysis, design with the new *SMT* method using the *C*offin shift, and design using the *SMT* method using the *M*odified Coffin shift. 47
4.3 Comparison between inelastic analysis and the SMT methods for larger strain ranges at a hold time of 100 hours. Methodologies are design by *I*nelastic analysis, design with the new *SMT* method using the *C*offin shift, and design using the *SMT* method using the *M*odified Coffin shift. 49
4.4 Comparison between inelastic analysis and the SMT methods for increasing hold times at a fixed strain range of 0.25%. Methodologies are design by *I*nelastic analysis, design with the new *SMT* method using the *C*offin shift, and design using the *SMT* method using the *M*odified Coffin shift. 49

1 Introduction

1.1 Overview

This report describes a new design method for high temperature creep-fatigue evaluation based on a combination of an elastic perfectly-plastic (EPP) analysis and design allowable curves constructed, conceptually, from Simplified Model Test (SMT) specimens. There are several goals in developing this new design method:

1. Avoid the empirical and overconservative damage diagram (D-diagram, creep-fatigue interaction diagram) approach currently used in Section III, Division 5 of the ASME Boiler and Pressure Vessel Code [1].

2. Simplify the process, when compared to current methods, of evaluating a structure against creep-fatigue damage.

3. Explicitly account for the effect of elastic follow up in the creep-fatigue design procedure.

The current methods in Section III of the ASME Code all rely on the D-diagram and therefore all may suffer from the over conservatism inherent in that approach. The simplified methods in the current Code – design by elastic analysis and design by elastic perfectly plastic analysis in Code Case N-862 [2] – treat follow up in an approximate, bounding, but very conservative way and may therefore overestimate the detrimental effect of follow up on creep-fatigue life. This new EPP+SMT approach aims to address both potential drawbacks of current methods while simplifying the process of evaluating creep-fatigue damage.

The new method combines several technologies developed through past work sponsored by the ART program. Extensive research and development has produced a specialized test specimen, the SMT specimen, that can directly assess the effect of elastic follow up on cyclic life [3, 4, 5, 6, 7]. The genesis for the approach was a paper written by one of the report authors on improved methods for creep-fatigue design [8]. Current work has developed a simpler testing method, the one bar SMT test, that can replicate tests previously required special specimens with a standard creep-fatigue sample. These tests can be used to establish the design data used in the EPP+SMT method or validate extrapolated design data.

The second component of the method is an analysis approach based on elastic perfectly-plastic analysis that accurately estimates the effective strain range at any point in a structure, approximately accounting for creep and plasticity [9]. This method allows a designer to bound these complicated material effects with a simple analysis procedure. Moreover, because elastic perfectly-plastic analysis does not require or store material state this method allows a designer to consider each individual load cycle independently and then afterwords superimpose results. This is an important aspect in practical design, as changing the definition of a single load cycle will not require reanalyzing the entire load history of the component. Moreover, the EPP approach uses the strain range established through a cyclic steady state shakedown type analysis, which means a designer only needs to run a handful of cycle repetitions to establish this steady-state response and not analyze the full load history of a component.

Section 4.2 describes the complete EPP+SMT method for uniaxial loading and a single load cycle definition. The final key components of the complete method are approaches

for applying the design data garnered through uniaxial tests to multiaxial strain states and multiple types of load cycles. These methods for the EPP+SMT approach are described in a companion report.

This report focuses on developing the design charts used as the acceptance criteria in the EPP+SMT approach. Essentially these are modified fatigue curves plotting an effective strain range versus the number of cycles to failure. Conventional fatigue diagrams account only for the effect of strain range and temperature. The EPP+SMT design charts additionally must account for the effect of hold time and elastic follow up, as quantified through a follow up factor. The SMT test methodology was developed specifically as an experimental test protocol that could independently control all four variables. However, SMT tests, like conventional creep-fatigue tests, cannot directly test the long holds at constant strain typical of operating structural components nor can they practically examine creep-fatigue for very small strain ranges. Both tests, while conceptually possible, would take a very long time to complete. Additionally, the EPP+SMT test method has only recently been developed and so the current test database is limited compared to the database of historical creep-fatigue tests. This report develops methods for extrapolating both SMT and creep-fatigue testing as a function of hold time and follow up factor. The methodologies developed here enable the practical use of the EPP+SMT method by expanding the design curve calibration database to creep-fatigue tests and by developing design curves accounting for the long hold times expected in operating components.

1.2 Elastic follow up

Elastic follow up quantifies the difference between a purely load controlled test and a purely strain controlled test. Figure 1.1 illustrates stress relaxation in three scenarios – pure load control, pure strain control, and mixed control – on both a stress versus strain plot and a stress versus time relaxation plot. Using this diagram, classically the elastic follow up factor is defined as

$$q = -\frac{\Delta\varepsilon_{creep}}{\Delta\varepsilon_{elastic}}. \tag{1.1}$$

With this definition a follow up factor of $q = 1$ indicates pure strain control while a follow up factor of $q = \infty$ indicates pure load control.

As Figure 1.1b indicates, higher values of elastic follow up tend to slow the rate of stress relaxation. Therefore, a material point undergoing relaxation at a higher value of follow up experiences higher stresses for longer times than a corresponding point relaxing from the same stress at a lower value of follow up. This mean increasing the follow up factor increases creep damage and tends to decrease creep-fatigue life. The SMT data summarized below demonstrates the correlation between follow up and decreased creep-fatigue cyclic life.

Follow up is significant to engineering design for two reasons. First, approximate analysis methods like elastic and elastic perfectly-plastic analysis cannot account for the stress/strain redistribution that causes elastic follow up. Therefore, these design methods attempt to account for follow up effects elsewhere in the design process. Traditionally, in the classical ASME design by elastic analysis approaches this is in load classification, where displacement-controlled stresses imposed through high values of elastic follow up are explicitly treated as primary loads when evaluating strain limits and creep-fatigue. Secondly, even in design by

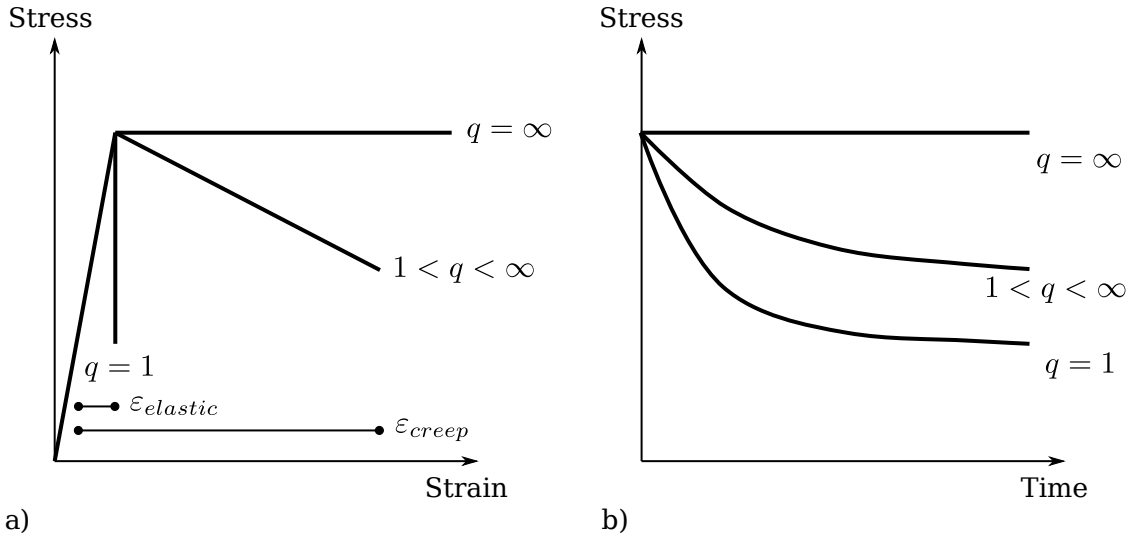

Figure 1.1: Schematic illustration of the effect of elastic follow up on the (a) stress/strain behavior and (b) stress/time behavior of an elastic-creep material undergoing stress relaxation.

inelastic analysis, which can explicitly account for the effects of follow up in the analysis step, designers often must introduce artificial cuts through the concept of a free-body diagram to couple structural systems in order to make design and analysis tractable. A classic example would be introducing an artificial interface between a vessel and nozzle and the attached piping system. While generalized boundary conditions are available, commonly this interface is either treated as either a traction or displacement boundary condition. With either approximation follow up across the interface is neglected.

And so an improved design method might better account for the effect of elastic follow up on creep-fatigue life. The EPP+SMT approach does this by quantifying cyclic life as a function of temperature, strain range, hold time, and follow up factor. This general design correlation can then be specialized to a particular value of follow up to account for the effect in an approximate, EPP analysis. The method proposed here bounds follow up by determining a representing bounding value of the follow up factor that represents the follow up typically found in advanced reactor structural components and specializing the general design correlation to this specific factor. An alternative approach might provide a means for estimating the value of the follow up factor at each point in a component and refer the designer to appropriate design charts accounting for that level of follow up.

2 Extrapolating data from SMT tests

2.1 Deformation

As described in the introduction, the available data SMT test data will need to be extrapolated out to reasonable operating hold times, cycle counts and, at least potentially, extrapolated to high values of the follow up factor. Current design methods already must extrapolate short hold times to realistic component loading periods, though sometimes the means of extrapolation is not obvious. The introduction noted that there is considerable difficulty interpreting the results from tests using the older Type 1 and Type 2 SMT specimens. In addition, while the experimental database has grow to be fairly extensive, at least for some materials, it only samples a relatively small portion of the complete four-dimensional data space spanned by the strain range, follow up factor, hold time, and temperature. The combination of all these factors complicates the process of determining a suitable extrapolation factor directly from the experimental data.

This section presents an alternative approach based on simple models. The idea is to apply several current models of creep-fatigue damage to a simplified model of an SMT test – essentially an elastic bar in series with a creeping bar – to determine the effect of follow up and hold time on the predicted cycles-to-failure for each model. These theoretical relations can then be examined to determine the form of a reasonable experimental extrapolation procedure.

Figure 2.1 illustrates the simple theoretical model used here. The two bar system consists of a elastic bar (2) in series with an elastic, perfectly-plastic, power law creep bar (1). Both bars have the same length and cross-sectional area. In this model the creeping bar is the test section, the elastic bar just provides the correct elastic follow up. The elastic constant of this bar will be specified in terms of the elastic follow up factor q. The figure also shows a representative stress-strain hysteresis loop for the creeping bar for a tensile hold. This figure assumes the applied strain range is sufficient to induce reversed plasticity in the gauge bar.

The simple extrapolation schemes here will calculate creep and fatigue damage based on a stable stress-strain hysteresis loop. This neglects the effect of creep-fatigue softening on the material's constitutive response, but means that all the different models of creep-fatigue damage use the same stable loop. The material properties of interest are the length l and cross-sectional area A of the two bars, the Young's modulus of the elastic bar E_2, which will be set as a function of the follow up factor q, and the Young's modulus E_1, flow stress $\sigma_0 = \frac{\Delta\sigma}{2}$, viscosity η, creep exponent $n > 1$, and time-independent backstress X of the gauge bar. The constitutive equations describing the response of each bar during a hold at fixed displacement δ, inducing a tensile stress greater than the backstress, are:

$$\dot{\varepsilon}_1 = \frac{\dot{\sigma}_1}{E_1} + \eta \left(\sigma_1 - X\right)^n \tag{2.1}$$

$$\dot{\varepsilon}_2 = \frac{\dot{\sigma}_2}{E_2}. \tag{2.2}$$

The equation of equilibrium is

$$\sigma_1 = \sigma_2 = \sigma \tag{2.3}$$

implying

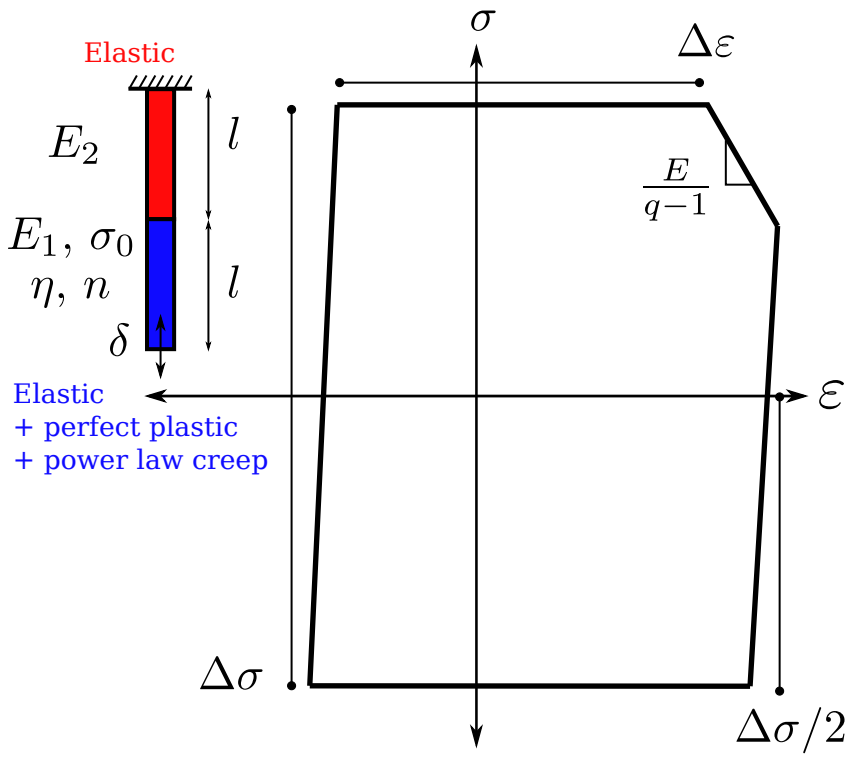

Figure 2.1: Schematic of the simple two bar model used to derive extrapolation formula for uniaxial creep-fatigue loading with follow up.

$$\dot{\sigma}_1 = \dot{\sigma}_2 = \dot{\sigma} \tag{2.4}$$

and the compatibility equation is

$$\dot{\varepsilon}_1 + \dot{\varepsilon}_2 = 0. \tag{2.5}$$

We define follow up as the ratio of the inelastic to the elastic work during the hold:

$$q = -\frac{\dot{W}_{creep}}{\dot{W}_{elastic}} = -\frac{\dot{\varepsilon}_{creep}}{\dot{\varepsilon}_{elastic}} \tag{2.6}$$

and so for the two bar system

$$q = -\frac{\dot{\varepsilon}_1 - \frac{\dot{\sigma}_1}{E_1}}{\frac{\dot{\sigma}_1}{E_1}} = 1 - E_1\frac{\dot{\varepsilon}_1}{\dot{\sigma}_1} = 1 + E_1\frac{\dot{\varepsilon}_2}{\dot{\sigma}_2} = 1 + E_1\frac{\frac{\dot{\sigma}_2}{E_2}}{\dot{\sigma}_2} = 1 + \frac{E_1}{E_2}. \tag{2.7}$$

So we can define the elastic modulus of the elastic bar as

$$E_2 = \frac{E_1}{q-1} \tag{2.8}$$

to set an arbitrary value of the follow up factor. Note the slope of the relaxation line on the hysteresis loop is

$$\frac{d\sigma}{d\varepsilon} = \frac{\dot{\sigma}_1}{\dot{\varepsilon}_1} = \frac{-\frac{\eta E_1}{q}\left(\sigma_1 - X\right)^n}{\frac{\dot{\sigma}_1}{E_1} + \eta\left(\sigma_1 - X\right)^n} = \frac{-\frac{\eta E_1}{q}\left(\sigma_1 - X\right)^n}{-\frac{\eta}{q}\left(\sigma_1 - X\right)^n + \eta\left(\sigma_1 - X\right)^n} = \frac{-\frac{E_1}{q}}{-\frac{1}{q}+1} = -\frac{E_1}{q-1} \tag{2.9}$$

Combining the constitutive, compatibility, and equilibrium equations with this definition of modulus gives the stress and strain in the gauge bar as the ordinary differential equations:

$$\dot{\sigma}_1 = -\frac{\eta E_1}{q}\left(\sigma_1 - X\right)^n \tag{2.10}$$

$$\dot{\varepsilon}_1 = \frac{\dot{\sigma}_1}{E_1} + \eta\left(\sigma_1 - X\right)^n \tag{2.11}$$

$$\dot{\varepsilon}_1 = \eta\left(\frac{q-1}{q}\right)\left(\sigma_1 - X\right)^n \tag{2.12}$$

with the initial condition

$$\sigma_1\left(0\right) = \sigma_0 = \frac{\Delta\sigma}{2} \tag{2.13}$$

The solution to Eq. 2.10 is

$$\sigma_1 = \left[\left(\sigma_0 - X\right)^{1-n} - \frac{\eta E_1\left(1-n\right)}{q}t\right]^{\frac{1}{1-n}} + X \tag{2.14}$$

For convenience from this point forward we drop the subscript 1 for the creeping bar so that:

$$\sigma = \left[\left(\sigma_0 - X\right)^{1-n} - \frac{\eta E\left(1-n\right)}{q}t\right]^{\frac{1}{1-n}} + X \tag{2.15}$$

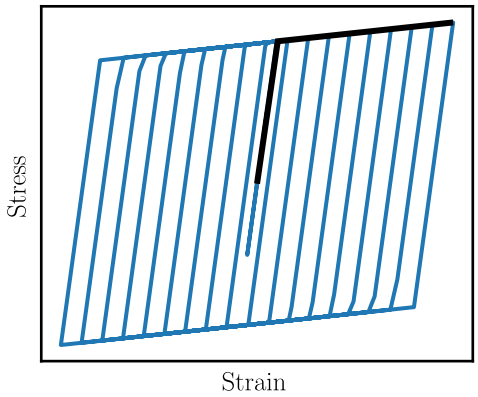

Figure 2.2: Example cyclic stress-strain curve. Notional results from a strain-controlled cyclic fatigue test with increasing strain range are plotted in blue. The resulting cyclic stress-strain curve is plotted in black.

for the stress relaxation in the gauge section. It will be convenient to define, for some hold time t_h,

$$\sigma_h = \left[(\sigma_0 - X)^{1-n} - \frac{\eta E (1-n)}{q} t_h \right]^{\frac{1}{1-n}} + X \tag{2.16}$$

and, via Eq. 2.11,

$$\varepsilon_h = \int_0^{t_h} \dot{\varepsilon} dt = \int_{\sigma_0}^{\sigma_h} \eta \left(\frac{q-1}{q} \right) (\sigma_1 - X)^n \frac{1}{\dot{\sigma}} d\sigma \tag{2.17}$$

$$\varepsilon_h = -\frac{q-1}{E} \int_{\sigma_0}^{\sigma_h} d\sigma = \frac{q-1}{E} (\sigma_0 - \sigma_h) \tag{2.18}$$

In the limit of $t_h \to \infty$ these expressions simplify considerably:

$$\sigma_h^\infty = X \tag{2.19}$$

$$\varepsilon_h^\infty = \frac{q-1}{E} (\sigma_0 - X) \tag{2.20}$$

For $\sigma_0 = \frac{\Delta\sigma}{2}$ there exists a closure relation between the stress range $\Delta\sigma$ and the strain range $\Delta\varepsilon$. This constitutive relation can be described by a cyclic stress-strain curve of the type shown in Figure 2.2 [10]. These cyclic stress-strain curves are typically measured using a series of fully-reversed strain controlled cyclic tests without holds – essentially a series of standard fatigue tests – in the manner described by the figure. For the purposes of deriving scaling relations we will assume some unknown functional relation $\Delta\sigma(\Delta\varepsilon)$. In general the map between a strain range and a constant, perfectly plastic flow stress $\Delta\sigma$ only applies in the limit of many repetitions of a prescribed cycle.

The preceding derivation assumes that the imposed strain will cause sufficient stress to induce plasticity during the rate independent portion and sufficient stress to exceed the backstress X during the hold portion of the cycle. These assumptions correspond to assuming the loading causes low cycle fatigue and non-negligible creep.

2.2 Damage

2.2.1 Methods using creep-fatigue interaction

This subsection discusses the effect of follow up on a model material with a failure time described by a creep-fatigue interaction equation. These types of models compute separate values of creep and fatigue damage and then combine the two according to some mathematical model, typically described with a diagram of the type shown in Fig. 2.3.

2.2.1.1 Fatigue damage

Typically, models of this type calculate fatigue damage using Miner's rule:

$$D_f = \frac{N}{N_f} \tag{2.21}$$

where N_f is the number of cycles to failure as a function of temperature and the effective strain range. As shown above, follow up increases the effective strain range so that if the range was $\Delta\varepsilon$ for strain-controlled loading it becomes $\Delta\varepsilon+\varepsilon_h$ with follow up. This expression provides a method for calculating the additional fatigue damage caused by follow up. In the limits of long holds, Eq. 2.20 above shows that the increased strain scales linearly with the quantity $q-1$.

2.2.1.2 Time-fraction with Larson-Miller extrapolation

The creep damage is given as the integral [1]

$$D_c = N\int_0^{t_h} \frac{dt}{t_f} \tag{2.22}$$

where t_f is the rupture time correlation to stress, typically at fixed temperature a power law:

$$D_c = N\int_0^{t_h} \frac{dt}{B\sigma^\beta}. \tag{2.23}$$

We can cast this as

$$D_c = -\frac{Nq}{B\eta E}\int_{\sigma_0}^{\sigma_h} \frac{d\sigma}{\sigma^\beta\left(\sigma - X\right)^n} \tag{2.24}$$

which is solvable in terms of standard functions only if $X = 0$:

$$D_c = -\frac{Nq}{B\eta E}\int_{\sigma_0}^{\sigma_h} \frac{d\sigma}{\sigma^{\beta+n}} = \frac{Nq}{B\eta E\left(\beta+n-1\right)}\left(\sigma_0^{-\beta-n+1} - \sigma_h^{-\beta-n+1}\right). \tag{2.25}$$

In the limits of long holds

$$D_c = \frac{Nq\sigma_0^{-\beta-n+1}}{B\eta E\left(\beta+n-1\right)} \tag{2.26}$$

and so creep damage is linear with the follow up, at least in this limit.

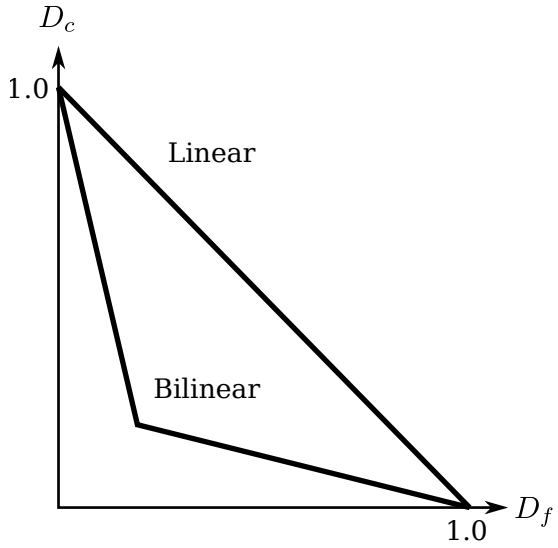

Figure 2.3: Notional creep-fatigue interaction diagrams illustrating the difference between a linear and a bilinear interaction.

The ASME code uses a bilinear creep-fatigue interaction diagram (see Fig. 2.3), so material failure is described by:

$$D_f + D_c = I \tag{2.27}$$

where I is a function of damage. Substituting Eqs 2.21, 2.25, and 2.27 gives a model for failure:

$$\frac{N}{N_f|_{\Delta\varepsilon+\varepsilon_h}} + \frac{Nq}{B\eta E\left(\beta+n-1\right)}\left(\left(\frac{\Delta\sigma}{2}\right)^{-\beta-n+1} - \sigma_h^{-\beta-n+1}\right) = I. \tag{2.28}$$

Explicitly solving this equation requires a fatigue curve, an interaction diagram, power law stress relaxation constants η and n, a log-linear Larson-Miller fit to rupture data described by A and α, the Young's modulus E, and a cyclic stress-strain curve relating $\Delta\varepsilon$ to $\Delta\sigma$. All this information except the latter can be extracted from the data in the ASME code:

1. the Code provides fatigue curves directly;
2. the Code provides the interaction diagram directly;
3. power law constants can be extracted by fitting isochronous stress-strain curve data, provided in the curve, in the vicinity of stress $\Delta\sigma/2$, strain $\Delta\varepsilon/2$, and over the time interval $[0, t_h]$;
4. the Larson-Miller parameters can be extracted to a local fit to the Code rupture stress data, S_r, over the stresses occurring during the relaxation cycle;
5. the Code provides the Young's modulus directly.

However, this leaves the cyclic stress-strain curve. As an approximation, this work uses the Code hot tensile curve to give a half-cycle $\frac{\Delta\varepsilon}{2} \rightarrow \frac{\Delta\sigma}{2}$ relation. This is a poor approximation

as it is well known that the cyclic stress-strain curve differs greatly from the monotonic stress-strain curve [11]. Future work could establish cyclic stress-strain curves for the Code materials to produce more accurate results.

Alternatively, we can assume some functional relation for the fatigue curve, interaction diagram, and cyclic stress strain curve and see what scaling relations Eq. 2.28 implies. Assume that the cyclic stress-strain curve can be described by a Ramberg-Osgood model:

$$\Delta\sigma = \left(\frac{\Delta\varepsilon}{K}\right)^{1/p}, \tag{2.29}$$

assume for low cycle fatigue the fatigue curve follows a power law relation,

$$N_f = A\Delta\varepsilon^{1/b}, \tag{2.30}$$

and assume a linear interaction relation

$$D_f + D_c = 1. \tag{2.31}$$

As described previously, the effect of follow up on fatigue is to add the extra strain due to follow up, ε_h, to the initial strain range $\Delta\varepsilon$ so that the strain range for calculating fatigue damage becomes $\Delta\varepsilon + \varepsilon_h$. Substituting these assumptions in Eq. 2.28 provides

$$N = \frac{A\left(\Delta\varepsilon + \varepsilon_h\right)^{1/b} B\eta E\left(\beta + n - 1\right)}{B\eta E\left(\beta + n - 1\right) + A\left(\Delta\varepsilon + \varepsilon_h\right)^{1/b} q\left(\left(\frac{\Delta\sigma}{2}\right)^{-\beta-n+1} - \sigma_h^{-\beta-n+1}\right)}. \tag{2.32}$$

In the limits of long hold times

$$\lim_{t_h\to\infty} N = \frac{A\left(\Delta\varepsilon + \frac{q-1}{E}\frac{1}{2}\left(\frac{\Delta\varepsilon}{K}\right)^{1/p}\right)^{1/b} B\eta E\left(\beta + n - 1\right)}{B\eta E\left(\beta + n - 1\right) + A\left(\Delta\varepsilon + \frac{1}{2}\frac{q-1}{E}\left(\frac{\Delta\varepsilon}{K}\right)^{1/p}\right)^{1/b} q\left(\left(\frac{1}{2}\left(\frac{\Delta\varepsilon}{K}\right)^{1/p}\right)^{-\beta-n+1}\right)}. \tag{2.33}$$

Assuming $B\eta E\left(\beta + n - 1\right) \ll A\left(\Delta\varepsilon + \frac{1}{2}\frac{q-1}{E}\left(\frac{\Delta\varepsilon}{K}\right)^{1/p}\right)^{1/b} q\left(\left(\frac{1}{2}\left(\frac{\Delta\varepsilon}{K}\right)^{1/p}\right)^{-\beta-n+1}\right)$ simplifies this to

$$\lim_{t_h\to\infty} N = \frac{B\eta E\left(\beta + n - 1\right)}{q\left(\left(\frac{1}{2}\left(\frac{\Delta\varepsilon}{K}\right)^{1/p}\right)^{-\beta-n+1}\right)} \tag{2.34}$$

which implies

$$N \propto \frac{1}{q\Delta\varepsilon^{1/p-\beta-n+1}} \tag{2.35}$$

which implies inverse scaling with q and some power law in $\Delta\varepsilon$. In the limit of low follow up:

$$\lim_{q\to 1} N = \frac{B\eta E\left(\beta + n - 1\right) A\Delta\varepsilon^{1/b}}{B\eta E\left(\beta + n - 1\right) + A\Delta\varepsilon^{1/b}\left(\left[\frac{1}{2}\left(\frac{\Delta\varepsilon}{K}\right)^{1/p}\right]^{-\beta-n+1} - \left(\left[\sigma_0^{1-n} - \eta E\left(1-n\right)t_h\right]^{\frac{1}{1-n}}\right)^{-\beta-n+1}\right)}. \tag{2.36}$$

Again assuming the $B\eta E\left(\beta+n-1\right)$ term is small gives

$$N \propto \frac{1}{\Delta\varepsilon^{1/p-\beta-n+1}+t_h^{\frac{1}{1-n}-\beta-n+1}} \tag{2.37}$$

which implies power law scaling for both $\Delta\varepsilon$ and t_h.

2.2.1.3 Ductility exhaustion

Creep damage is given as the integral [12]:

$$D_c = N\int_0^{t_h}\frac{\dot{\varepsilon}_{cr}}{\varepsilon_R}dt \tag{2.38}$$

Assuming a fixed ductility:

$$D_c = \frac{N}{\varepsilon_R}\int_0^{t_h}\eta\left(\sigma-X\right)^n dt = \int_{\sigma_0}^{\sigma_h}\eta\frac{\left(\sigma-X\right)^n}{-\frac{\eta E}{q}\left(\sigma_1-X\right)^n}d\sigma = \frac{Nq}{E\varepsilon_R}\left(\sigma_0-\sigma_h\right). \tag{2.39}$$

In the limits of a long hold:

$$D_c = \frac{Nq}{E\varepsilon_R}\left(\sigma_0-X\right) \tag{2.40}$$

which shows that in this limit creep damage scales linearly with the follow up factor.

Typically, ductility exhaustion methods use a linear creep-fatigue interaction diagram (see Fig. 2.3), meaning the condition

$$D_f + D_c = 1 \tag{2.41}$$

describes material failure. Substituting Eqs. 2.21, 2.39, and 2.41 gives an expression for the number of cycles to failure:

$$N = \frac{E\varepsilon_R\, N_f|_{\Delta\varepsilon+\varepsilon_h}}{E\varepsilon_R + q\left(\frac{\Delta\sigma}{2}-\sigma_h\right)N_f|_{\Delta\varepsilon+\varepsilon_h}}. \tag{2.42}$$

Given material failure data from tests without follow up, a cycle stress-strain curve, and a power law description of the material's stress relaxation behavior this equation can be used to calculate design curves that directly account for the effect of strain range, hold time, and follow up factor on the cyclic life of a specimen under reversed uniaxial load.

Alternatively, we can assume functional relations for the cyclic stress-strain curve and fatigue curve to looking at the scaling relation implied by this equation. Assume that the cyclic stress-strain curve can be described by a Ramberg-Osgood model:

$$\Delta\sigma = \left(\frac{\Delta\varepsilon}{K}\right)^{1/p} \tag{2.43}$$

and assume for low cycle fatigue the fatigue curve follows a power law relation

$$N_f = A\Delta\varepsilon^{1/b}. \tag{2.44}$$

These equations can be substituted into Eq. 2.42 to give an analytic model:

$$N\left(\Delta\varepsilon, q, t_h\right) = \frac{E\varepsilon_R A\left(\Delta\varepsilon + \varepsilon_h\right)^{1/b}}{E\varepsilon_R + q\left(\frac{1}{2}\left(\frac{\Delta\varepsilon}{K}\right)^{1/p} - \sigma_h\right)\left(\Delta\varepsilon + \varepsilon_h\right)^{1/b}}.$$

For long hold times and without a backstress this expression becomes:

$$\lim_{t_h\to\infty} N = \frac{E\varepsilon_R A\left(\Delta\varepsilon + \frac{q-1}{E}\sigma_0\right)^{1/b}}{E\varepsilon_R + \frac{q}{2}\left(\frac{\Delta\varepsilon}{K}\right)^{1/p}\left(\Delta\varepsilon + \frac{q-1}{E}\sigma_0\right)^{1/b}}.$$

Assuming the $E\varepsilon_R$ term is small

$$N \propto \frac{1}{q\Delta\varepsilon^{1/p}} \tag{2.45}$$

which implies that in the limit of long hold times the number of cycles to failure scales inversely to q and as a power law in $\Delta\varepsilon$.

In the limit of low values of follow up and without a backstress:

$$\lim_{q\to 1} N = \frac{E\varepsilon_R A\Delta\varepsilon^{1/b}}{E\varepsilon_R + \left(\frac{1}{2}\left(\frac{\Delta\varepsilon}{K}\right)^{1/p} - \left[\sigma_0^{1-n} - \eta E\left(1-n\right)t_h\right]^{\frac{1}{1-n}}\right)\Delta\varepsilon^{1/b}}. \tag{2.46}$$

Again ignoring constant prefactors:

$$N \propto \frac{1}{\Delta\varepsilon^{1/p} + t_h^{\frac{1}{1-n}}} \tag{2.47}$$

which implies that the number of cycles to failure scales as separate power laws in the strain range and hold time.

2.2.2 A unified method: dissipated work

An alternative approach could develop scaling relations by assuming that the cyclic life is proportional to the energy dissipated as work during cyclic deformation. This concept was discussed in the early years of research into creep-fatigue [13], but has not been carried through into a design code. Figure 2.4 illustrates the effect of follow up on the energy dissipated in each hysteresis cycle.

The total work is

$$W = W_{base} + W_{hold} + W_q \tag{2.48}$$

Neglecting elastic deformation, the work of the cycle without any follow up or hold time is

$$W_{base} = \Delta\sigma\Delta\varepsilon. \tag{2.49}$$

The work caused by a hold at constant strain is

$$W_{hold} = \frac{1}{2E}\left(\frac{\Delta\sigma}{2} - \sigma_h\right)\left(\frac{\Delta\sigma}{2} - \sigma_h\right) + \frac{1}{E}\left(\Delta\sigma - \frac{\Delta\sigma}{2} + \sigma_h\right)\left(\frac{\Delta\sigma}{2} - \sigma_h\right) = \frac{1}{E}\left(\frac{3\Delta\sigma^2}{8} - \frac{\sigma_h\Delta\sigma}{2} - \frac{\sigma_h^2}{2}\right). \tag{2.50}$$

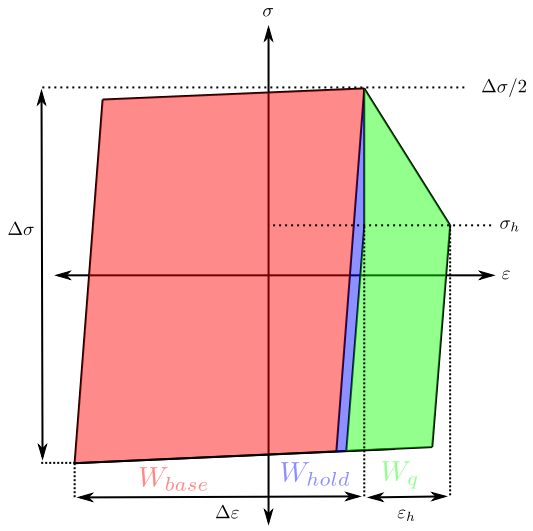

Figure 2.4: Schematic showing the partitioning of dissipated energy into fatigue (W_{base}), creep-fatigue (W_{hold}), and follow up (W_q) contributions.

The work caused by follow up is

$$W_q = \frac{q-1}{E}\left(\frac{3\Delta\sigma^2}{8} - \frac{\Delta\sigma\sigma_h}{2} - \frac{\sigma_h^2}{2}\right). \tag{2.51}$$

The work due to a strain hold can be combined with the work due to follow up to give

$$W_{qh} = \frac{q}{E}\left(\frac{3\Delta\sigma^2}{8} - \frac{\Delta\sigma\sigma_h}{2} - \frac{\sigma_h^2}{2}\right). \tag{2.52}$$

Clearly then the work due to follow up scales linearly with the follow up factor.

The total work, ignoring the backstress, is

$$W = \Delta\sigma\Delta\varepsilon + \frac{q}{E}\left(\frac{3\Delta\sigma^2}{8} - \frac{\Delta\sigma}{2}\left[\left(\frac{\Delta\sigma}{2}\right)^{1-n} - \frac{\eta E\,(1-n)}{q}t_h\right]^{\frac{1}{1-n}} - \frac{1}{2}\left[\left(\frac{\Delta\sigma}{2}\right)^{1-n} - \frac{\eta E\,(1-n)}{q}t_h\right]^{\frac{2}{1-n}}\right). \tag{2.53}$$

Making the assumption that the cyclic stress/strain curve coincides with the monotonic hot tensile curves given the ASME code, the dissipated work can be calculated from Code data following the process outlined above.

Alternatively, assuming a Ramberg-Osgood relation between strain range and stress range, this expression can be viewed as a polynomial giving the work in terms of

$$W \propto P\left(\Delta\varepsilon, q, t_h\right) \tag{2.54}$$

where P expresses some arbitrary polynomial relation between the listed variables, including cross terms of arbitrary order. Most work-based damage models for fatigue assume the number of cycles to failure will be inversely proportional to the total dissipated work raise to some power [14]:

$$N \propto \frac{1}{W^r}$$

and so (absorbing the power r into the general polynomial)

$$N \propto \frac{1}{P\left(\Delta\varepsilon, q, t_h\right)} \tag{2.55}$$

Note this form is the general case of the forms derived from the time fraction (Eq. 2.37) and ductility exhaustion (Eq. 2.47) models described previously.

3 Preliminary design curves

3.1 Scaling directly from experimental data

The previous chapter suggests that some polynomial in the three variables

$$N = \frac{1}{P\left(\Delta\varepsilon, q, t_h\right)} \tag{3.1}$$

may reasonably predict the number of cycles to failure from experimental data, given the follow up factor, strain range, and hold time at fixed temperature.

Previous ART sponsored work has developed various testing methodologies for including follow up in cyclic creep-fatigue type tests [7, 15, 6, 4, 5]. The majority of these experiments tested Alloy 617 samples. As was described in the introduction, the results of previous tests on Type 1, Type 2, YSMT, and pressured SMT specimens are difficult to interpret. However, this database of 25 tests is the most extensive collection of data, to our knowledge, explicitly exploring the effect of follow up on creep-fatigue life. Additionally, ART sponsored work on the ASME Alloy 617 Code Case has produced numerous standard fatigue and creep-fatigue tests. These tests fall into the general design curve framework described in the introduction. For fatigue tests $q = 1$ and $t_h = 0$ while for creep-fatigue tests $q = 1$ and the other parameters are determined by the test protocol.

The majority of the specialized SMT tests are at 950° C and so this section attempts to apply Eq. 2.55 to fitting and extrapolating the total experimental database at this temperature. As described both in Chapters 1 and 4 one part of the EPP+SMT design methodology is consistently calculating the test strain range and the strain range in the actual component using the same EPP methodology. In order to do this here we ran simulations of the Type 1 and Type 2 SMT tests using the EPP analysis methodology described in previous reports [9] and detailed below. The standard fatigue and creep-fatigue tests are fully strain controlled and so the relevant strain range is simply the range applied during the test. The complete database consists of 93 tests, listed in Appendix A.

After some experimentation, a modification to Eq. 3.1 adequately fits the low cycle fatigue data in the database. The experiments using a strain range of 0.3% do not follow the same trend and, at least for standard tests without follow up, seem to fall into a separate high cycle fatigue regime. For the moment these data points are excluded from the database. First consider a variant of Eq. 3.1:

$$N = \frac{1}{q}\frac{C}{\Delta\varepsilon}\left(\frac{1}{1+t_h}\right)^p. \tag{3.2}$$

This expression is interesting for two reasons:

1. For $q = 1$ it is a Coffin model [16], essentially modifying a standard $N = \frac{C}{\Delta\varepsilon}$ equation for the fatigue curve by a factor accounting for the frequency of loading. Though not used in the current ASME Code, this approach of modifying fatigue curves to account for hold time was used in previous version of the Code.

2. The equation can be fit sequentially. First the constant C can be determined from fatigue data. Then p can be determined from creep-fatigue data. Finally, no additional

Parameter	Value	Units
C	8.34	%
p	4.91	-

Table 3.1: Parameters for the base Coffin model (Eq. 3.2).

Parameter	Value	Units
C	8.34	%
p	36.24	-
D	0.832	-

Table 3.2: Parameters for the modified Coffin model (Eq. 3.3).

data is required to account for follow up, as the relation postulates a simple inverse scaling relation for the effect of follow up on cyclic life.

Table 3.1 lists the best-fit parameters for this model, when applied to the Alloy 617 database. Figure 3.1 compares the model to the experimental data. This model exaggerates the effect of hold time on cyclic life, essentially postulating that with infinite hold time the cyclic life of the sample would decrease to zero. However, as Figure 3.1a shows the actual experimental data shows saturation with increasing hold time: a creep-fatigue test with a hold time of 30 minutes fails in about the same number of cycles as a test with a 10 minute hold. Stress relaxation explains hold time saturation. For long enough holds the stress in the samples relaxes to a point where the sample accumulates negligible creep damage. This happens quite quickly for Alloy 617 at 950° C.

A modified Coffin relation captures hold time saturation:

$$N = \frac{1}{q}\frac{C}{\Delta\varepsilon}\frac{\left(\frac{1}{1+t_h}\right)^p + D}{1+D} \tag{3.3}$$

where D can be determined from creep-fatigue test data (along with p). Table 3.2 lists the calibrated parameters for this version of the model and Figure 3.2 compares the model predictions to experimental data. Given the general uncertainty in creep-fatigue experiments, the model reasonably captures the experimental trend (average relative error for cycles to failure is 22.0%). However, Figure 3.3 shows that the model fails to capture the test results for low strain ranges of 0.3% or less.

A third version of the model would allow for some general inverse power law dependence on the follow up factor:

$$N = \frac{1}{q^a}\frac{C}{\Delta\varepsilon}\frac{\left(\frac{1}{1+t_h}\right)^p + D}{1+D}. \tag{3.4}$$

Including the extra exponent, a, in the model produces a negligible increase in accuracy and the calibrated value of a is approximately 1.0. This experiment strongly suggests that cyclic life does scale inversely with q. The challenge is to develop an accurate representation of the effect of hold time on cyclic life.

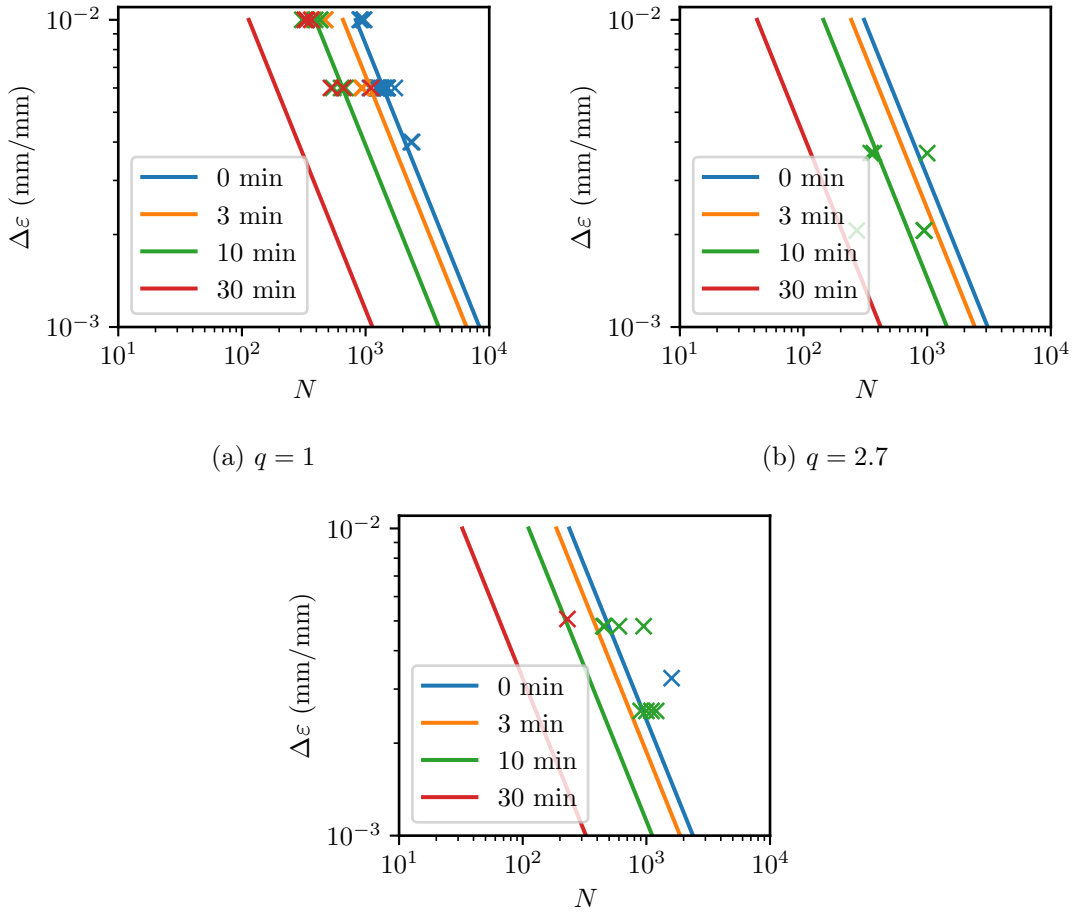

(a) $q = 1$

(b) $q = 2.7$

(c) $q = 3.5$

Figure 3.1: Design curve fit to experimental Alloy 617 data at 950° C using the base Coffin model (Eq. 3.2).

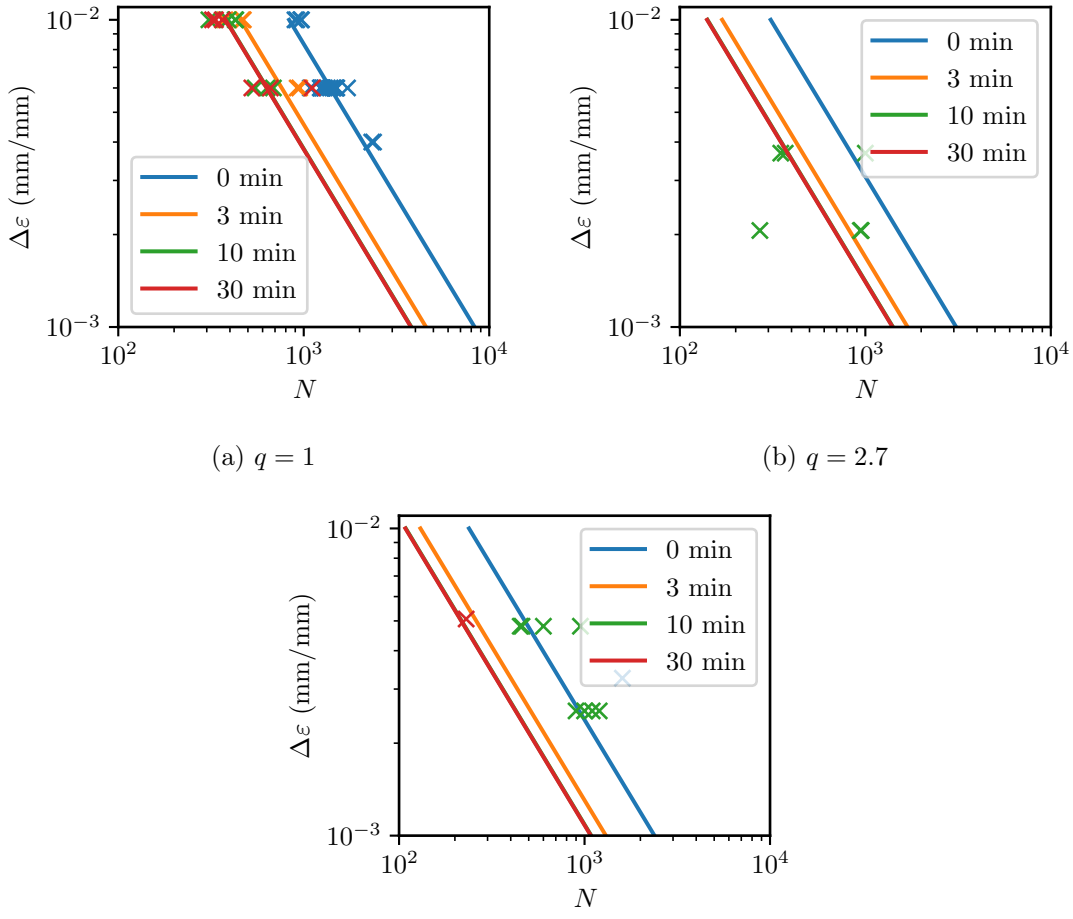

(a) $q = 1$

(b) $q = 2.7$

(c) $q = 3.5$

Figure 3.2: Design curve fit to experimental Alloy 617 data at 950° C using the modified Coffin model (Eq. 3.3). The red and green lines overlap.

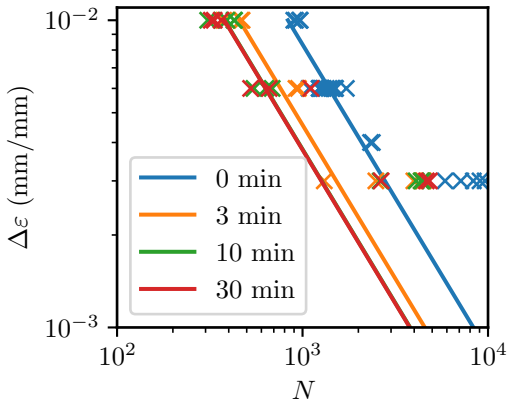

Figure 3.3: The modified Coffin model (Eq. 3.3) with the parameters given in Table 3.2 compared to the full Alloy 617 dataset for $q = 1$, including the small strain range data. The red and green lines overlap.

Finally, a pragmatic approach to capturing the lower strain range data is to shift the base fatigue curve by the factor predicted by Eq. 3.3:

$$N_{SMT} = N_{fatigue} \left\{ \frac{1}{q} \frac{\left(\frac{1}{1+t_h}\right)^p + D}{1+D} \right\}. \tag{3.5}$$

Figure 3.4 plots the nominal design curves predicted by this approach for 950° C compared to the experimental data. This approach combines an accurate representation of fatigue life with a good accounting of the effect of hold time and follow up.

The approaches described in this Chapter rely on experimental data to directly constrain the model used to create design curves. An alternative approach uses existing databases of design data, for example the data contained in the ASME Code, to construct SMT-type design curves.

3.2 Constructing design curves from Code data

3.2.1 Time fraction

Essentially, this Section uses Eq. 2.28 and the ASME design data to construct EPP+SMT design curves. However, rather than computing creep damage using the analytically expression derived above, which assumes a power law relation between stress and rupture time, this Section instead uses Eq. 2.15, substituting $X = 0$, to calculate a stress relaxation profile starting from $\Delta\sigma/2$ and then uses the ASME time-fraction approach to calculate creep damage from that stress relaxation profile (Eq. 2.22).

The required data with this approach are isochronous curves, from which to fit a local power law creep model, fatigue curves, a creep rupture correlation, and an interaction diagram. This section considers two types of correlations: curves using average material data, in order to validate the approach against the Alloy 617 experimental data, and design curves

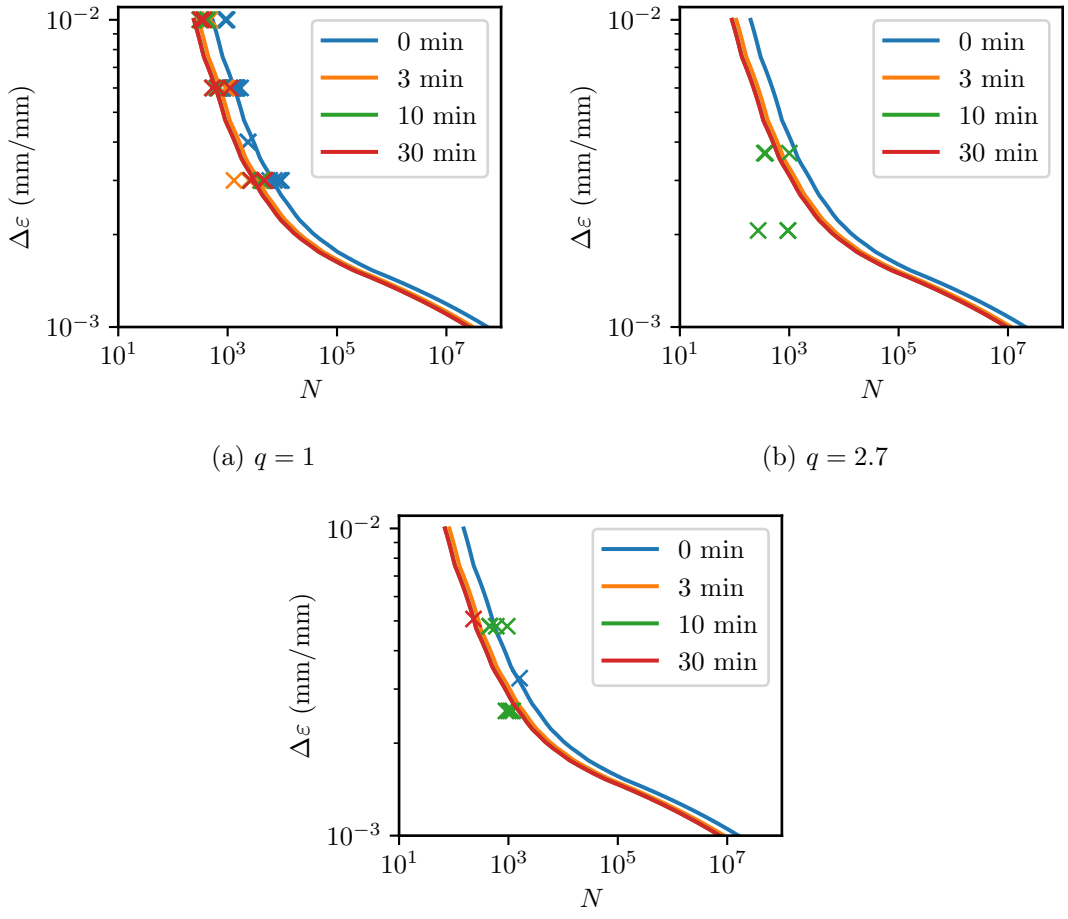

(a) $q = 1$

(b) $q = 2.7$

(c) $q = 3.5$

Figure 3.4: Design curve constructed by shifting the nominal ASME fatigue curve by the Coffin-shift predicted by (Eq. 3.3). The red and green lines overlap.

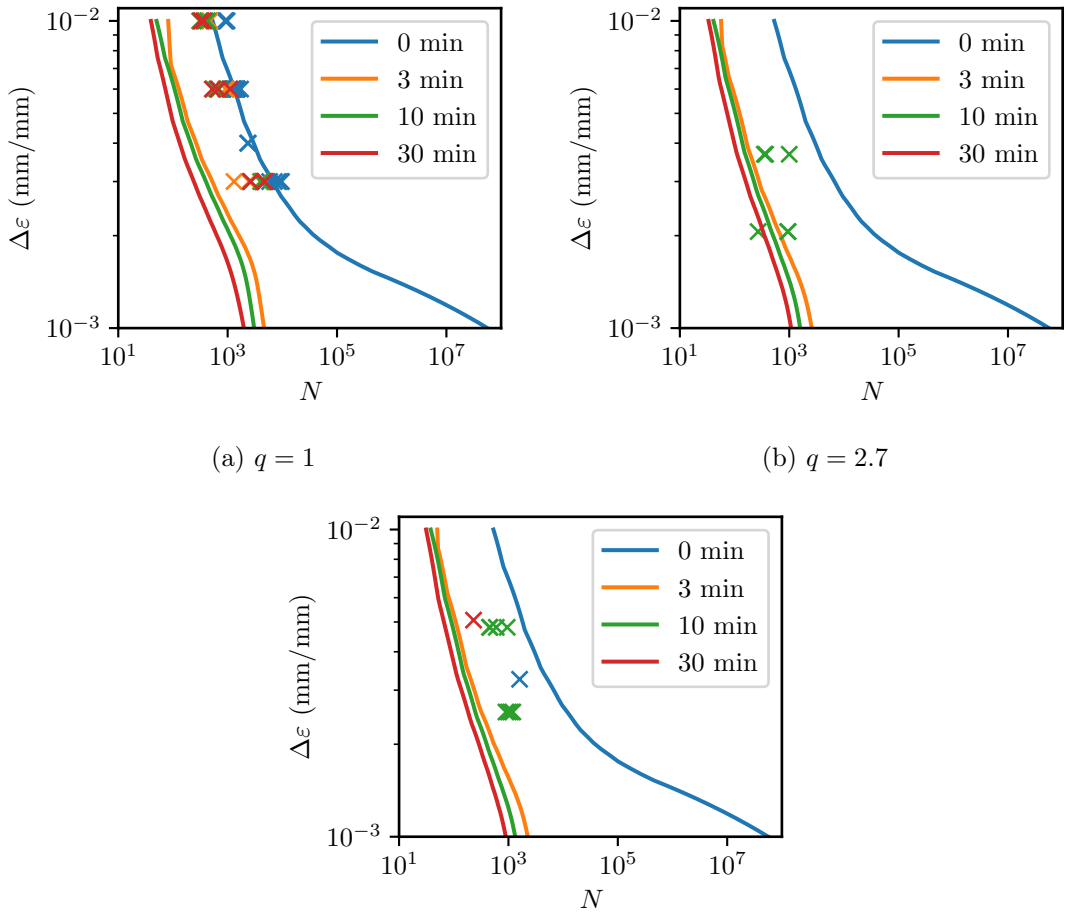

(a) $q = 1$

(b) $q = 2.7$

(c) $q = 3.5$

Figure 3.5: EPP+SMT design curves for Alloy 617 at 950° C constructed with nominal material properties using the time-fraction approach and the ASME database compared to the experimental data.

using minimum properties and the design factors from the ASME Code. The calculations for the average response uses the average fatigue curves and the average Larson-Miller rupture correlation from the background documents to the Alloy 617 Code Case currently under consideration at the ASME. The design curves use the actual Code Case (for Alloy 617) or Section III, Division 5 design fatigue curves and rupture stress correlations. The isochronous curves and interaction diagram notionally represent an average material response and so both sets of calculations uses this information from the ASME Code Case without modification.

Figure 3.5 compares the average property curves to the Alloy 617 experimental data, now including the data for small strain ranges. For pure fatigue the curve closely matches the experimental data, which it should as the fatigue data here was used to calibrate the ASME Code Case fatigue curves. This approach overestimates the effect of hold time on cyclic life, which is a conservative design approximation. The assumption that the creep strain follows a power law relation during stress relaxation may contribute to this overestimate –

it may be that the power law underestimates stress relaxation. However, more likely is that the ASME approach, even stripped of design margin, is overconservative. The most likely culprit is the interaction diagram. Even though this diagram notionally represents an average material response, many of the creep-fatigue data fall above the Code Case interaction diagram, meaning that the Code Case diagram is overconservative for some cases. The constructed curves are likewise overconservative compared to the data for $q > 1$. However, this conservatism may simply reflect the general conservatism of the ASME method for hold time effects, rather than reflect conservatism in model for the effect of follow up.

One of the main purposes of developing this new method for evaluating creep-fatigue damage is to avoid some of the overconservatism in the current Code rules and in particular to avoid using a creep-fatigue interaction diagram. The approach used in this section of course propagates the overconservatism of the D-diagram approach into the EPP+SMT design curves. As more SMT test data becomes available this data should be used to construct new design curves, following the process outlined in the previous section. However, the approach developed here provides a method for developing trial design data for the new approach from the existing design database. These preliminary curves can be used to test the new method as additional SMT test data is collected.

This approach can be used to calculate design curves for any of the Class A ASME materials and to generate curves for realistic plant hold times. Furthermore, this method can be used to generate EPP-SMT design curves that are consistent with the design margin contained in the current ASME Code. Figures 3.6-3.8 provide such design curves for Alloy 617 for several combinations of temperature and follow up factor. Figures 3.9-3.11 provide similar curves for 316H.

Overall, these prospective preliminary design curves show a strong effect of hold time and a much smaller effect of follow up. In fact, the general approximation of "divide the number of cycles to failure by the follow up factor" is reasonable at the high temperatures and lower strain ranges, where creep damage dominates fatigue damage. However, dividing by, for example $q = 2$, only produces a small effect on a log-scale plot. Note that the effect of hold time is more significant for small strain ranges. At high strain ranges the fatigue damage governs the life fraction calculation, whereas for lower strain ranges fatigue damage is negligible and creep can significantly impact the number of cycles to failure. Because follow up directly affects creep and not fatigue, the regions dominated by creep damage, here small strain ranges, will be more affected by an increase in elastic follow. However, as described previously, the hold time effect postulated by the ASME relations may be overconservative.

3.2.2 Work-based

The previous subsection illustrates the difficulty in constructing design curves for a novel creep-fatigue design method using existing experimental databases. Using this approach the new method will naturally pick up the defects of the old method, in this case the conservatism embedded in the ASME creep-fatigue interaction diagram. The only alternatives are to:

1. Base the extrapolation off a perfect model of creep-fatigue. An example might be some method of calculating creep damage that leads to a consistent creep-fatigue interaction diagram – i.e. results from all creep-fatigue tests fall along a single line. However, the existence of a perfect creep-fatigue correlation would, at least partly, obviate this work.

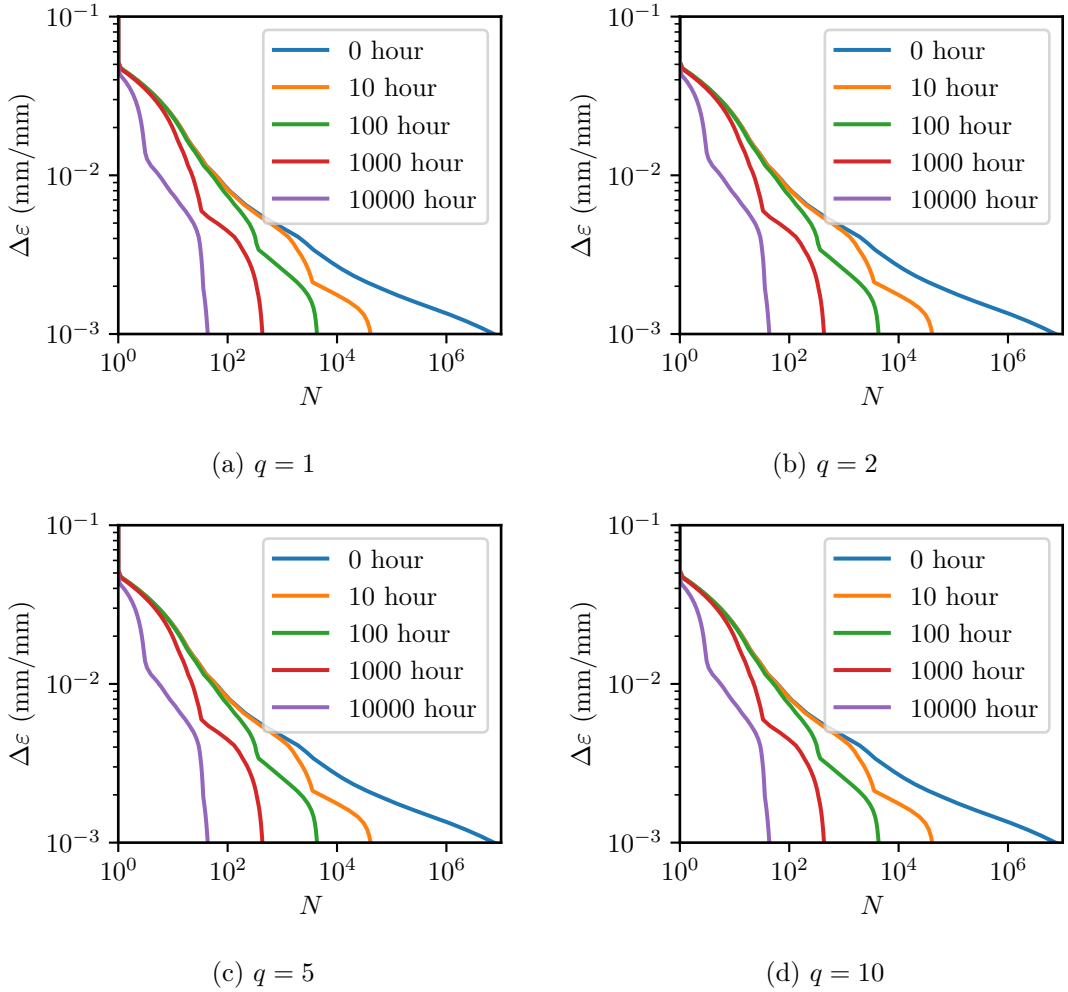

(a) $q = 1$

(b) $q = 2$

(c) $q = 5$

(d) $q = 10$

Figure 3.6: Design curves constructed with the time-fraction approach from the ASME design data for Alloy 617 at $T = 500°$ C.

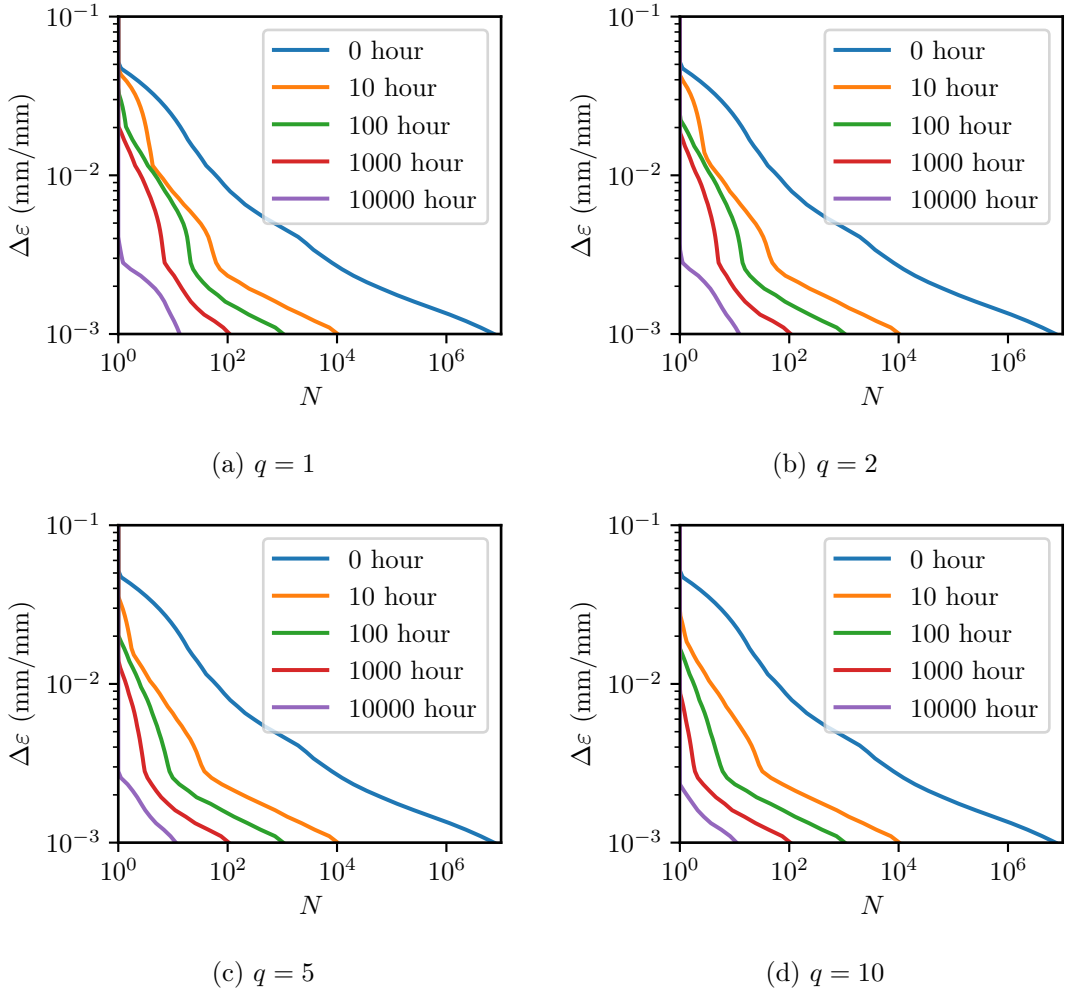

(a) $q = 1$

(b) $q = 2$

(c) $q = 5$

(d) $q = 10$

Figure 3.7: Design curves constructed with the time-fraction approach from the ASME design data for Alloy 617 at $T = 700°$ C.

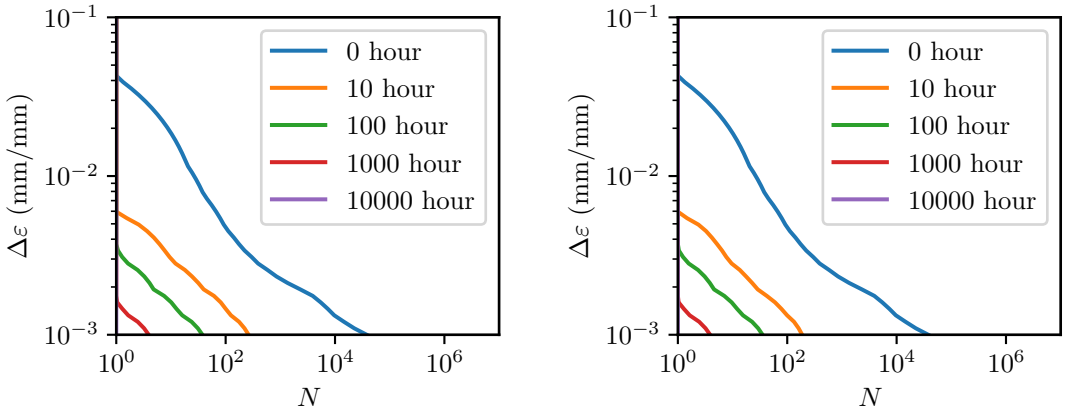

(a) $q = 1$

(b) $q = 2$

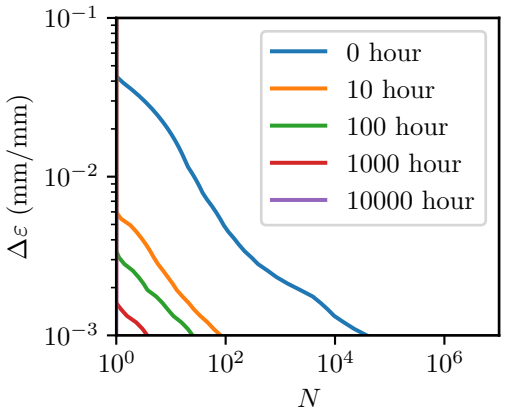

(c) $q = 5$

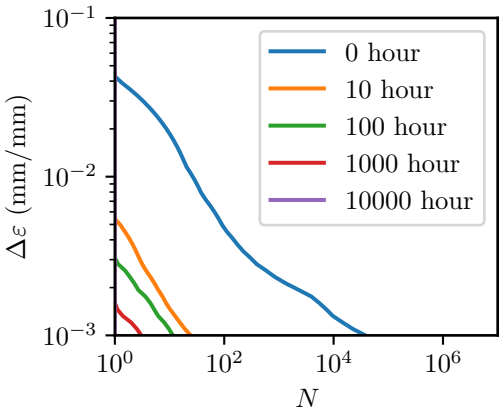

(d) $q = 10$

Figure 3.8: Design curves constructed with the time-fraction approach from the ASME design data for Alloy 617 at $T = 900°$ C. The 10,000 hour hold curve is off the plot, the material cannot survive even a single cycle with that length of hold.

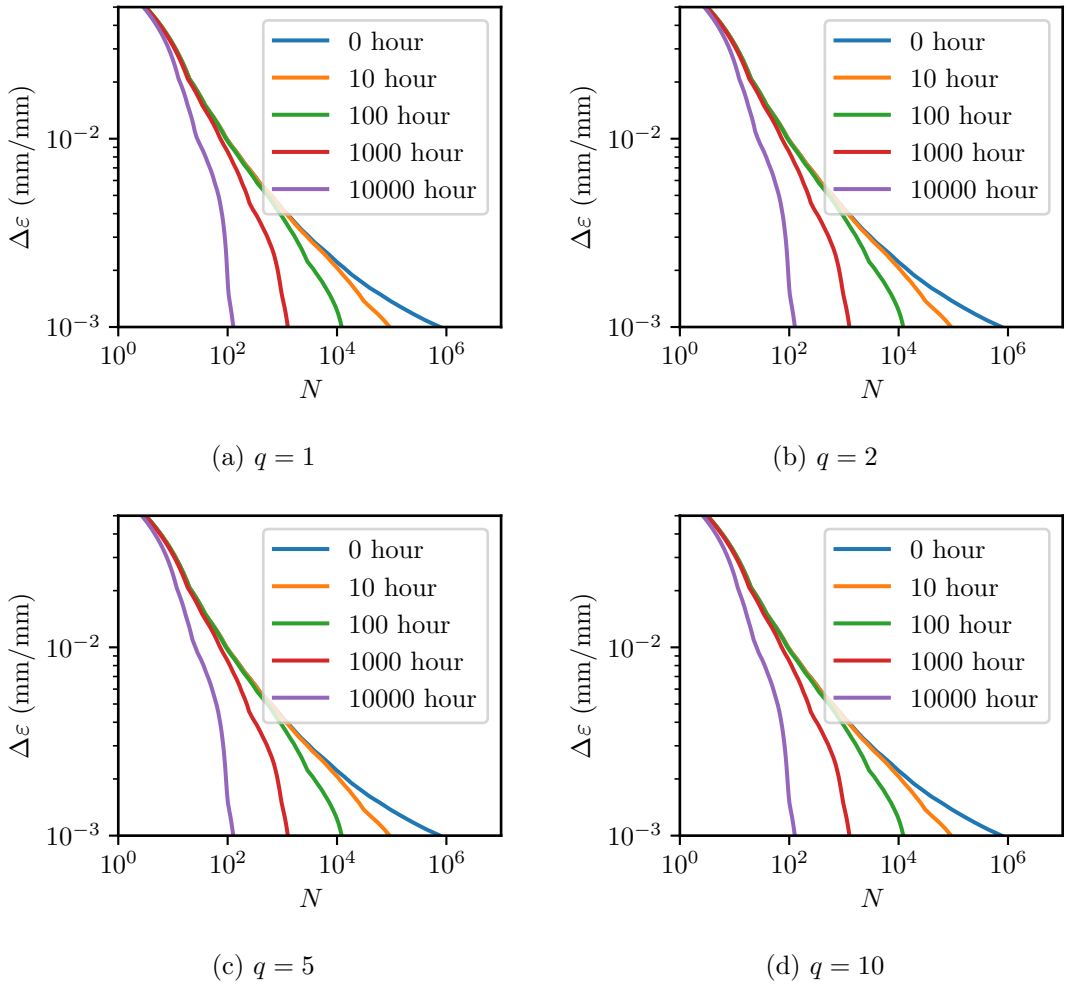

(a) $q = 1$ (b) $q = 2$

(c) $q = 5$ (d) $q = 10$

Figure 3.9: Design curves constructed with the time-fraction approach from the ASME design data for 316H at $T = 500°$ C.

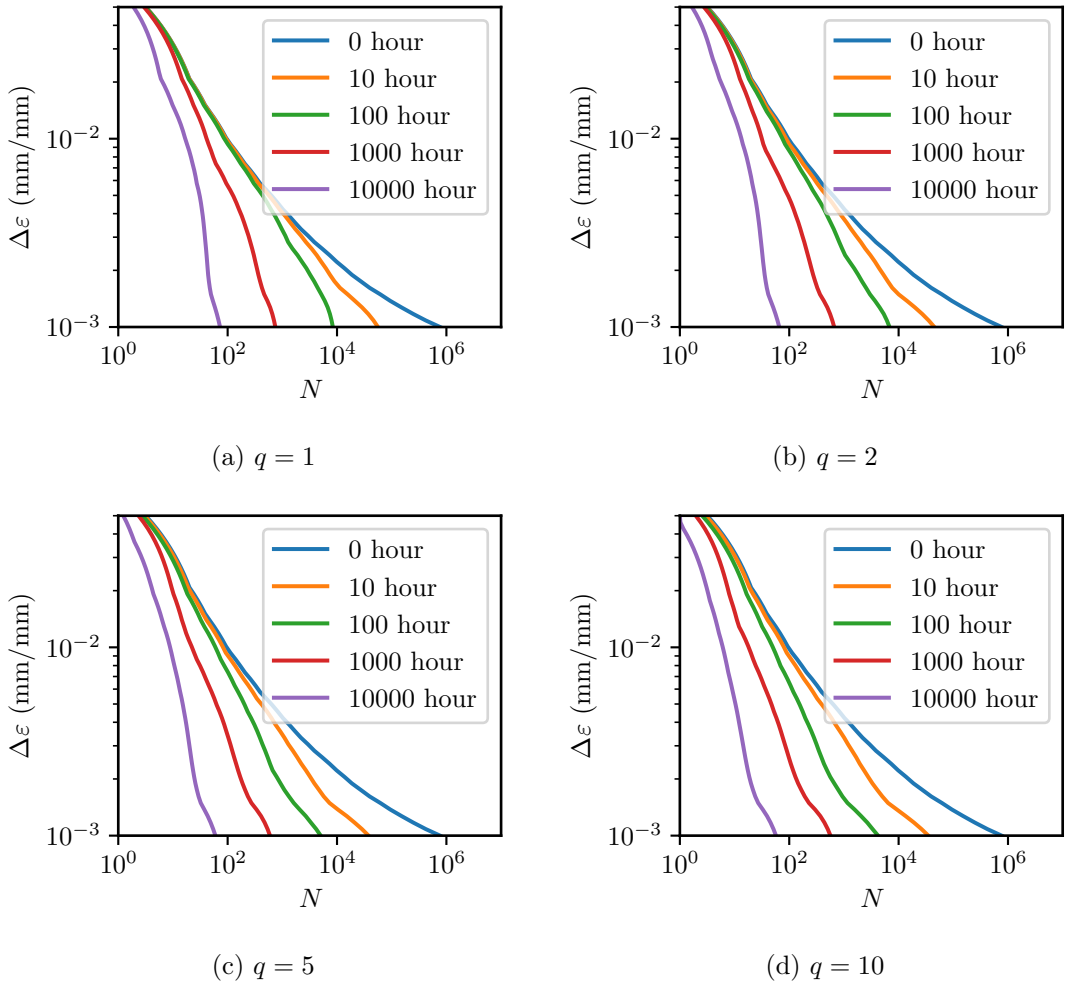

(a) $q = 1$ (b) $q = 2$

(c) $q = 5$ (d) $q = 10$

Figure 3.10: Design curves constructed with the time-fraction approach from the ASME design data for 316H at $T = 575°$ C.

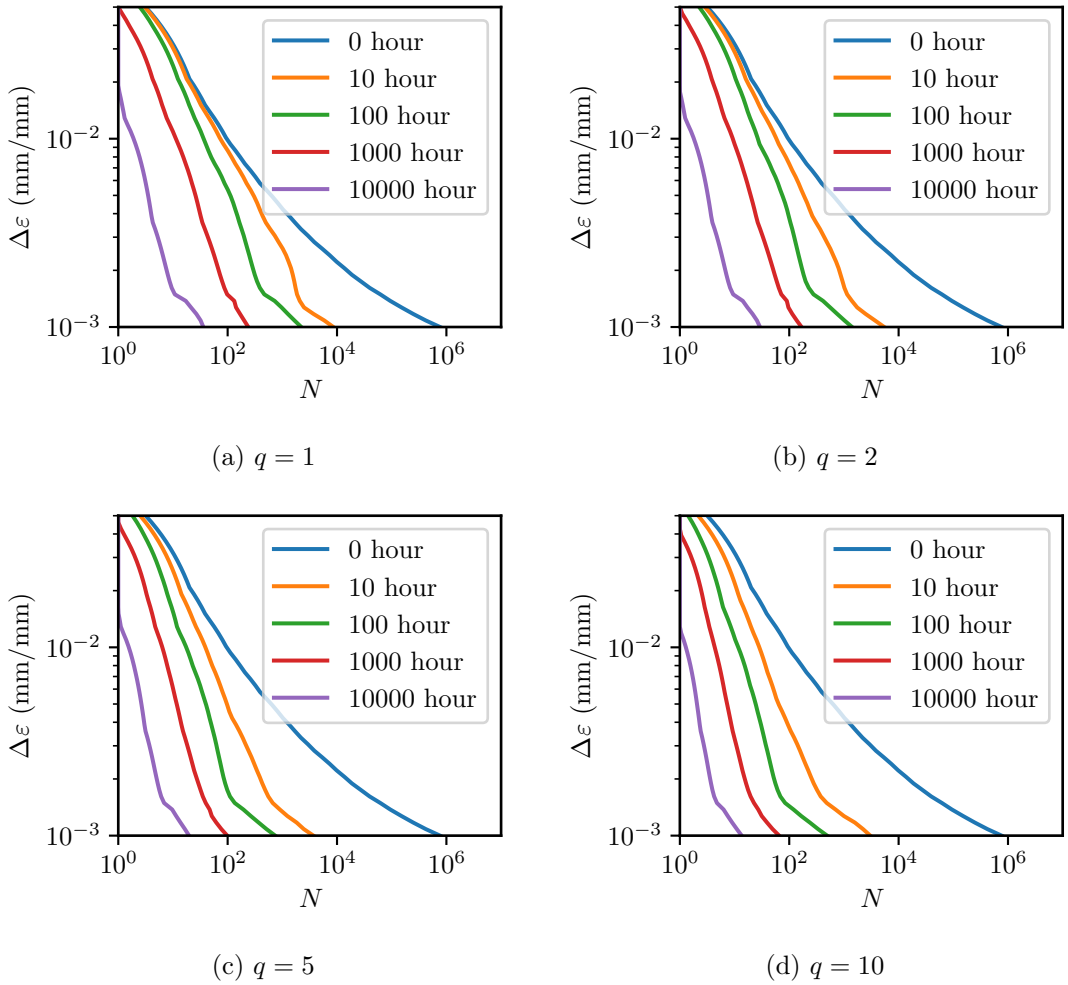

(a) $q = 1$ (b) $q = 2$

(c) $q = 5$ (d) $q = 10$

Figure 3.11: Design curves constructed with the time-fraction approach from the ASME design data for 316H at $T = 650°$ C.

2. Develop a new extrapolation method that has not been adopted by an existing design code.

The previous work has demonstrated that the problem for the EPP+SMT method is mostly in accounting for the effect of hold time. Given an accurate representation of the effect of hold time on cyclic life, dividing the number of cycles to failure by the follow up factor may adequately account for the experimentally-measure effect of elastic follow up.

This subsection explores the hypothesis that the energy dissipated by inelastic work during a test predicts failure for general creep-fatigue loading conditions. The challenge with this hypothesis is that reconstructing the total dissipation requires a record of the complete stress-strain hysteresis for a series of tests. This data is extremely difficult to find for past studies because it was impossible to easily report this data before the advent of the internet and widespread digital storage – printing such a record of a single test requires reams of paper. However, the DOE-NE sponsored work on the Alloy 617 Code Case did produce complete stress-strain-time data for a large series of tests on that material.

For creep-fatigue tests (or creep-fatigue plus follow-up tests, like the SMT method) given a complete stress-strain history of the test the dissipated energy is

$$W = \int \sigma d\varepsilon. \tag{3.6}$$

Figures 3.12 (for 850° C) and Fig. 3.13 (for 950° C) explore the hypothesis that the cyclic life can be predicted by a power relation between the inelastic work per cycle

$$W_{avg} = \frac{W}{N}. \tag{3.7}$$

These figures plot W_{avg} versus N on a log scale. Subfigure (a) colors the points based on the hold time t_h and subfigure (b) colors the points based on the strain range $\Delta\varepsilon$. If the hypothesis holds then the points should form a straight line in log space and there should be no contrary trend in terms of strain range or hold time. This correlation fails both criteria: the trend is not particularly linear and there is a definite contrary trend in terms of hold time, especially evident on the 850° C plot.

Consider an alternate hypothesis: that cyclic life scales as a power law with a corrected work by cycle given by

$$W_{corr} = W\frac{C\Delta\varepsilon/\dot{\varepsilon} + t_h}{t_{total}} \tag{3.8}$$

where $\dot{\varepsilon}$ is the test strain rate, t_{total} is the total test time, and C is a constant to be determined. Note that if $C = 1$ then

$$W_{corr} = W\frac{\Delta\varepsilon/\dot{\varepsilon} + t_h}{t_{total}} = W\frac{t_{cycle}}{t_{total}} = \frac{W}{N} = W_{avg}. \tag{3.9}$$

One way to think about this expression for $C > 1$ is that it implies that work dissipated during rate-independent plastic deformation is more damaging than work done by creep during a hold at fixed strain. The constant C is a temperature-dependent material parameter.

Figures 3.14 (for 850° C) and Fig. 3.15 (for 950° C) test this hypothesis by plotting the corrected work against cycles to failure on a log scale, again coloring the points to check for

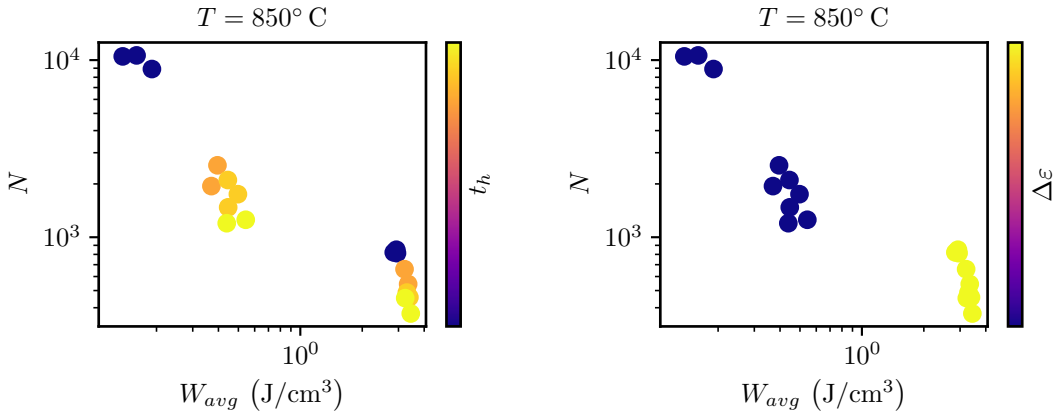

(a) Points colored by hold time.

(b) Points colored by strain range.

Figure 3.12: Correlation between work-per-cycle (W_{avg}) and cycles to failure (N) for the 850° C Alloy 617 data.

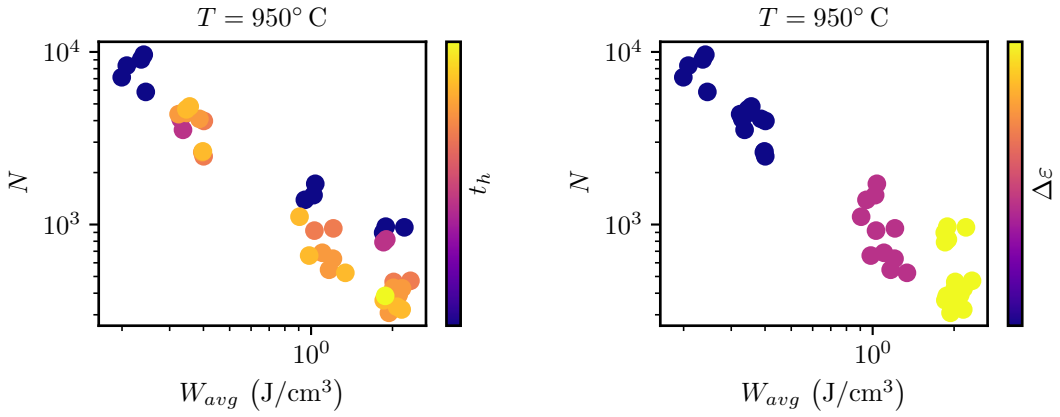

(a) Points colored by hold time.

(b) Points colored by strain range.

Figure 3.13: Correlation between work-per-cycle (W_{avg}) and cycles to failure (N) for the 950° C Alloy 617 data.

T (°C)	C
850	3.177
950	5.376

Table 3.3: Optimal values of C for the corrected work predictor.

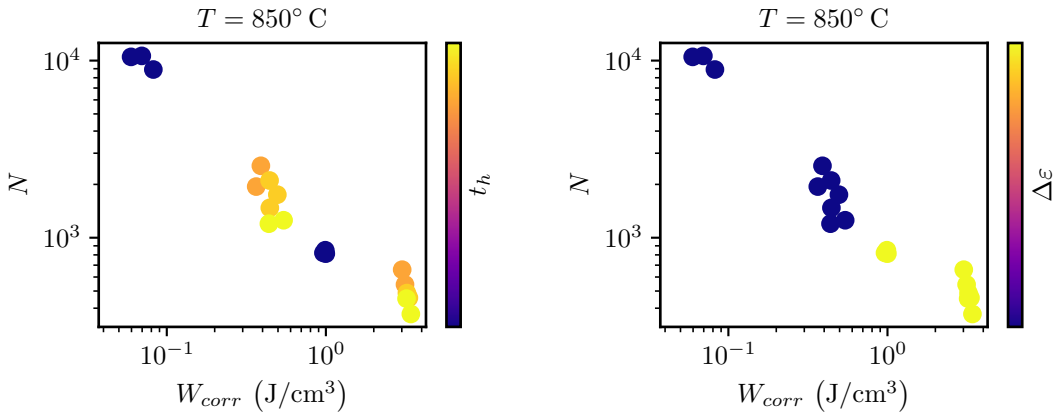

(a) Points colored by hold time.

(b) Points colored by strain range.

Figure 3.14: Correlation between corrected work-per-cycle (W_{corr}) and cycles to failure (N) for the 850° C Alloy 617 data.

any contrary correlations with hold time or strain range. These plots use the temperature-specific optimal values of C, listed in Table 3.3, that produce the best log-linear correlation. The corrected work is a much better predictor of cyclic life than the average work per cycle. In particular, the model fits the data at 950° C quite well and produces no apparent contrary correlations in strain range or time. One advantage of this model is that $C = 0$ indicates the negligible creep temperature – the temperature at which stress relaxation does not damage the material.

Casting the corrected-work model into plots of cyclic life versus temperature, strain range, and follow up requires a model for the actual work dissipated per cycle $W_{cycle}(\Delta\varepsilon, q, T)$. Equations 2.48, 2.49, and 2.52 provide such a model, when combined with the cyclic stress-strain curve and power law stress relaxation constants assumed from the ASME Code, following the method described above. Crucially, the Code creep-fatigue interaction diagram is not required to build the EPP-SMT design curves. Potentially then this method may avoid the overconservatism inherent in the interaction diagram.

Note that

$$W_{corr} = W_{cycle} N \frac{C\Delta\varepsilon/\dot{\varepsilon} + t_h}{N\left(\Delta\varepsilon/\dot{\varepsilon} + t_h\right)} = W_{cycle} \frac{C\Delta\varepsilon/\dot{\varepsilon} + t_h}{\Delta\varepsilon/\dot{\varepsilon} + t_h} \tag{3.10}$$

which only involves hysteresis loop data. The best-fit correlation to the A617 data at 950° C is

$$N = \Gamma W_{corr}^{\gamma} \tag{3.11}$$

for $\Gamma = 939.4$, $\gamma = -1.226$, and $C = 5.376$ and times and strain rates in terms of seconds. The analysis here assumes a strain rate of $\dot{\varepsilon} = 0.005\,\mathrm{s}^{-1}$, which matches the Alloy 617

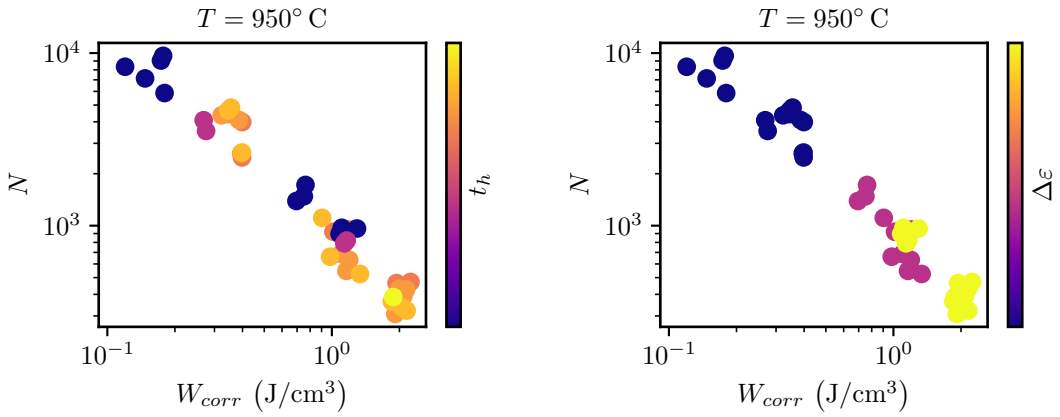

(a) Points colored by hold time.

(b) Points colored by strain range.

Figure 3.15: Correlation between corrected work-per-cycle (W_{corr}) and cycles to failure (N) for the 950° C Alloy 617 data.

experimental data.

Figure 3.16 compares the A617 nominal design curves calculated with this approach to the SMT experimental data. The standard fatigue curve ($q = 1$ and $t_h = 0$) underpredicts the actual experimental data. This implies that Eqs. 2.48, 2.49, and 2.52 underestimate the amount of work dissipated in the cycle or that the model is inadequate. This makes sense as this method does not account adequately account for changes in the cyclic flow stress — recall the cyclic stress-strain curve was approximated by the uniaxial stress-strain curve. This model predicts a smaller and more quickly saturating effect of hold time when compared to the other methods described previously.

The corrected-work correlation shows promise, but implementation would require a better method for bounding the dissipated work over some cyclic life. A modified EPP method may provide an adequate bound.

3.2.3 Coffin-shift to design fatigue curves

A final approach combines the Code data and a limited set of additional test data. The concept is to start with ASME Code fatigue curves, including design margin, and shift the curves to account for hold time and follow up effects using either Eq. 3.2 or Eq. 3.3. Calibrating the unsaturating or saturating Coffin parameters requires access to standard creep-fatigue results – strain range, temperature, and hold time mapped to cycles to failure. This data is widely available. In addition, a few SMT tests would be needed to validate the $1/q$ scaling assumed by the models.

Figure 3.17 plots shifted design curves for Alloy 617 at 950° C using the unsaturating Coffin model parameters determined in the previous chapter. Note that the combined affect of the ASME design factors and the aggressive hold time shift combine to make the model predict zero life for holds greater than 1 hour. Figure 3.18 plots similar curves using the saturating Coffin model. As discussed above, the standard Coffin model is very conservative compared to the Alloy 617 at 950° C, whereas the modified Coffin model is quite accurate.

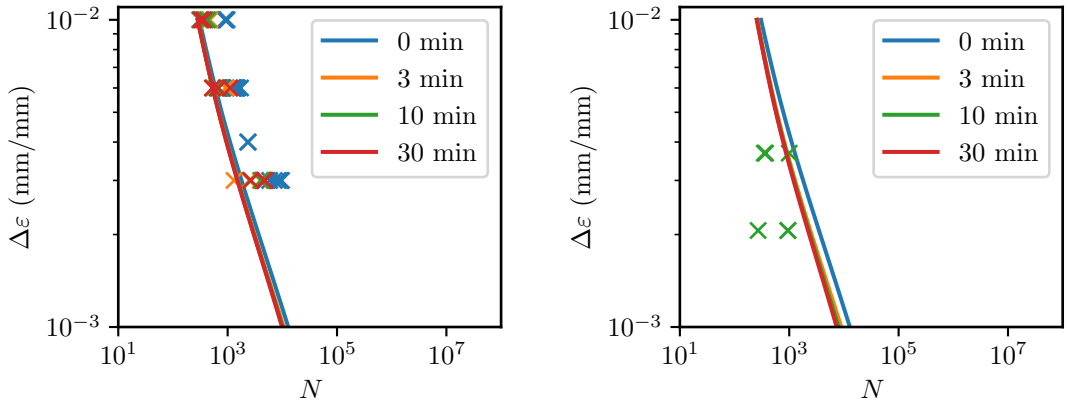

(a) $q = 1$

(b) $q = 2.7$

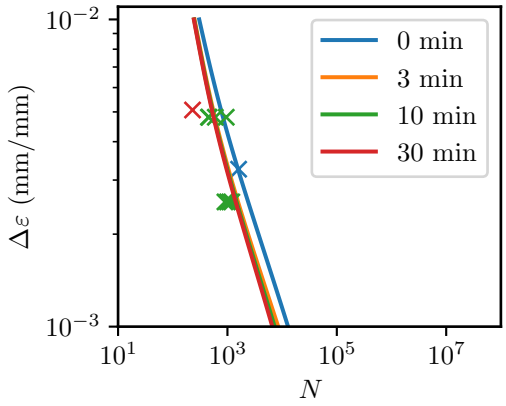

(c) $q = 3.5$

Figure 3.16: EPP+SMT design curves for Alloy 617 at 950° C constructed with nominal material properties using work-based approach compared to the experimental data.

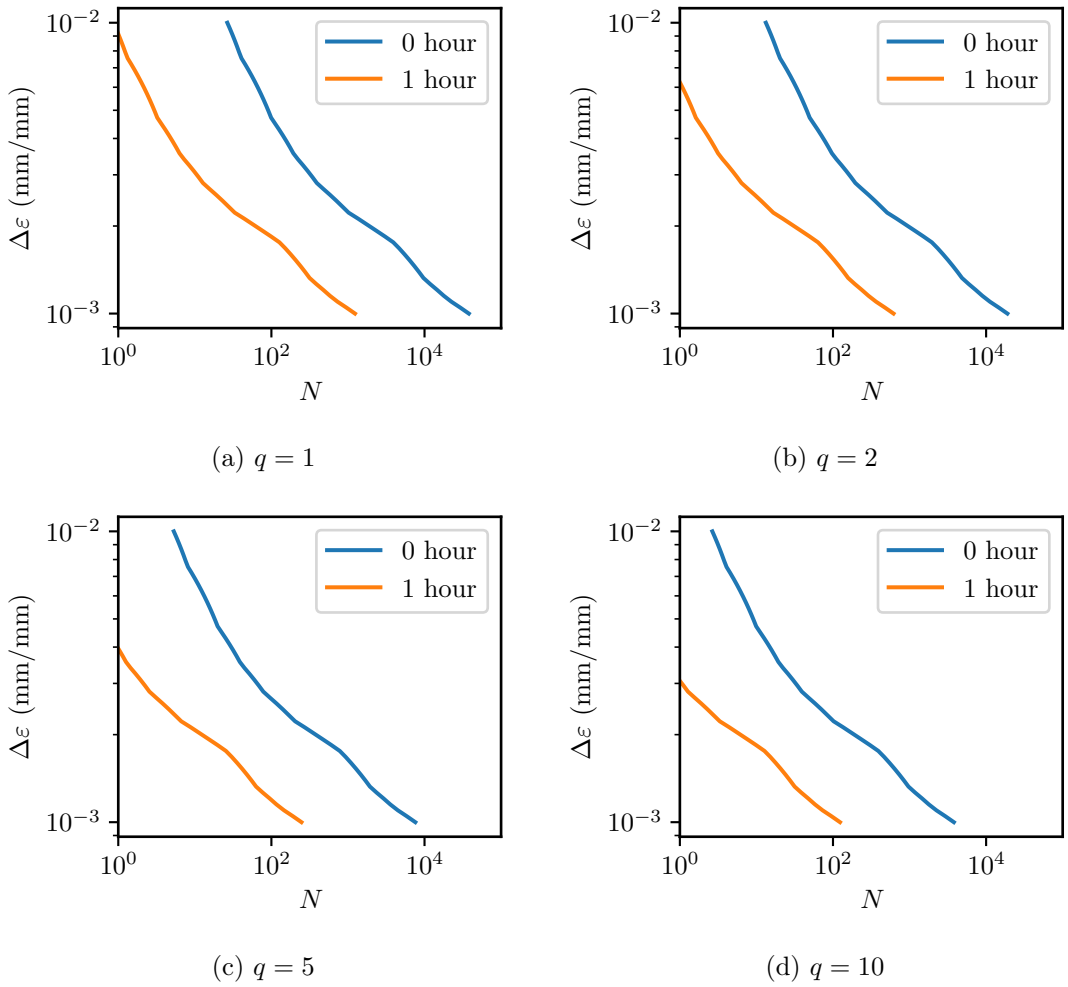

(a) $q = 1$

(b) $q = 2$

(c) $q = 5$

(d) $q = 10$

Figure 3.17: Design curves constructed with the standard Coffin shift starting from the Alloy 617 design fatigue curves at $T = 950°$ C.

However, additional test data will be required to determine if this trend holds true at lower temperatures where creep is slower. The potential concern is that the modified model, calibrated to the available relatively short hold time creep-fatigue test data, will predict hold time saturation too early. This would make the approach non-conservative for realistic long hold periods. This concern can be addressed simply by taking the available creep-fatigue test database at lower temperatures and different materials, calibrating the modified Coffin model, extrapolating out to long hold times, and assessing the results.

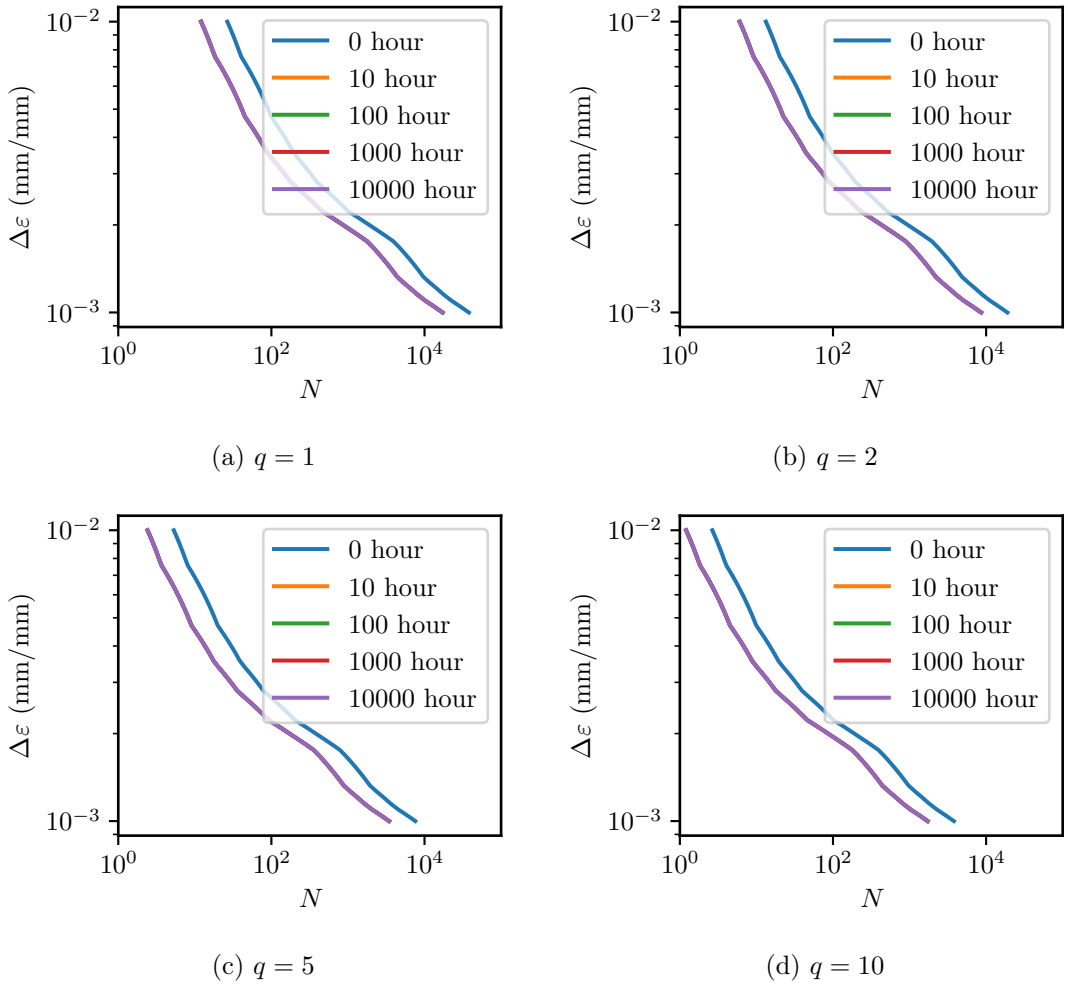

(a) $q = 1$

(b) $q = 2$

(c) $q = 5$

(d) $q = 10$

Figure 3.18: Design curves constructed with the saturating, modified Coffin shift starting from the Alloy 617 design fatigue curves at $T = 950°$ C.

4 Creep-fatigue design method for uniaxial loading

4.1 Additional design curves

The previous chapter describes a method for determining design curves for the new creep-fatigue design method that does not require an extensive database of specialized tests with follow up. This means it is possible to assemble design curves using the test database underlying the current ASME methods. Of course, some SMT-type tests will need to be performed to validate the follow up effect predicted by the simple $1/q$ rule.

As an example, this Section constructs design curves for Grade 91 steel. An ASME Standards Technology, LLC report summarizes the fatigue and creep-fatigue testing database for this material [17]. Following the approach described in the previous chapter, Figure 4.1 shows standard and modified Coffin shift fits to the experimental data at 538° C. Figure 4.2 shows similar plots at 593° C.

From these calibrated shifts, Figures 4.3 and 4.4 (538° C) and Figs. 4.5 and 4.6 (593° C) show design curves for Grade 91 for various follow up factors, calculated with the method described in Subsection 3.2.3 above.

Obviously the base and modified Coffin approaches give very different design curves, particularly for long hold times. As designed, the modified approach predicts a saturating effect of hold time representing the effect of stress relaxation in the material. The critical question is if the modified approach is accurately extrapolating the short hold time creep rupture tests out to realistic hold times. If the modified model predicts premature saturation it could lead to unsafe designs. In the absence of long hold time creep-fatigue tests data, the only way the conservatism of the modified and standard shifts can be assessed is through a comparison to existing design methods. This process first requires detailing the complete prospective design procedure for the new approach.

As described in the introduction, the final step in fixing design curves for the EPP+SMT method will be selecting a bounding value of follow up factor representative of discontinuities in operating high temperature structural components. This value of follow up is yet to be determined. However, reasonable values for gross structural discontinuities range from 2 to 4 and reasonable values of local stress concentrations range from 5 to 10. Potentially, separate design curves could be used to assess creep-fatigue near notches to account for local notch effects.

4.2 Uniaxial design method

This section describes the complete proposed design method for one type of loading cycle and for uniaxial deformation. A companion report discusses extending this basic methodology to account for multiaxial loading and the effect of combined load cycles. The EPP methodology for calculating the strain range was described in a previous report [9].

The uniaxial, uniform cycle design method is defined by the following procedure:

1. Determine the cyclic thermal and mechanical loads on the component from the design specification and an appropriate thermal analysis.

2. From this load history, determine an appropriate hold time, t_h, representative of the time the component remains under constant external mechanical and thermal loads.

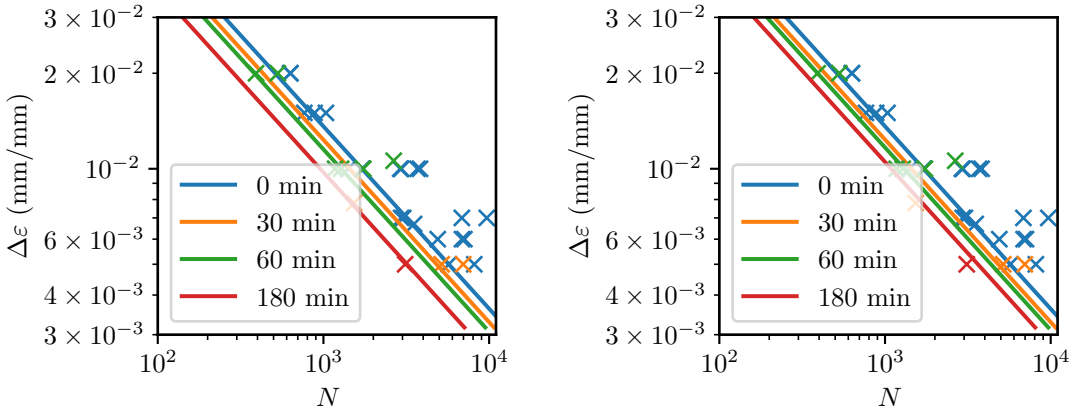

Figure 4.1: (a) Coffin and (b) modified Coffin shifts fit to the experimental Grade 91 fatigue and creep-fatigue data at 538° C.

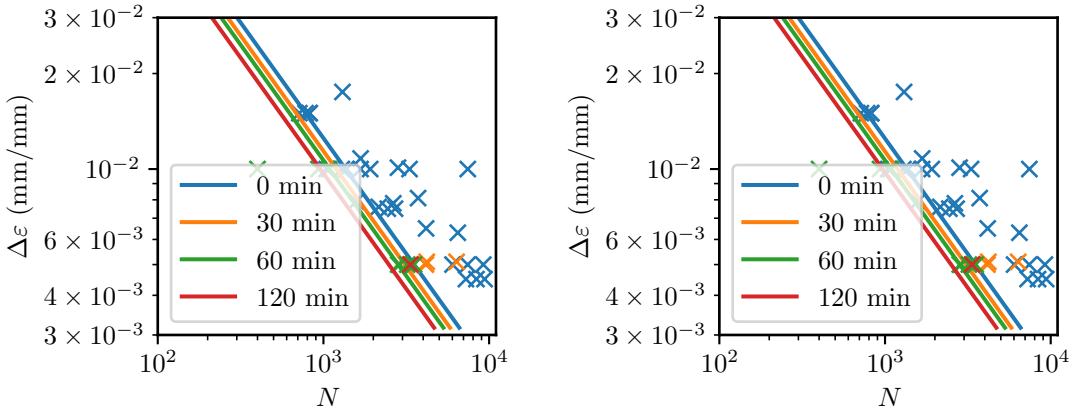

Figure 4.2: (a) Coffin and (b) modified Coffin shifts fit to the experimental Grade 91 fatigue and creep-fatigue data at 593° C.

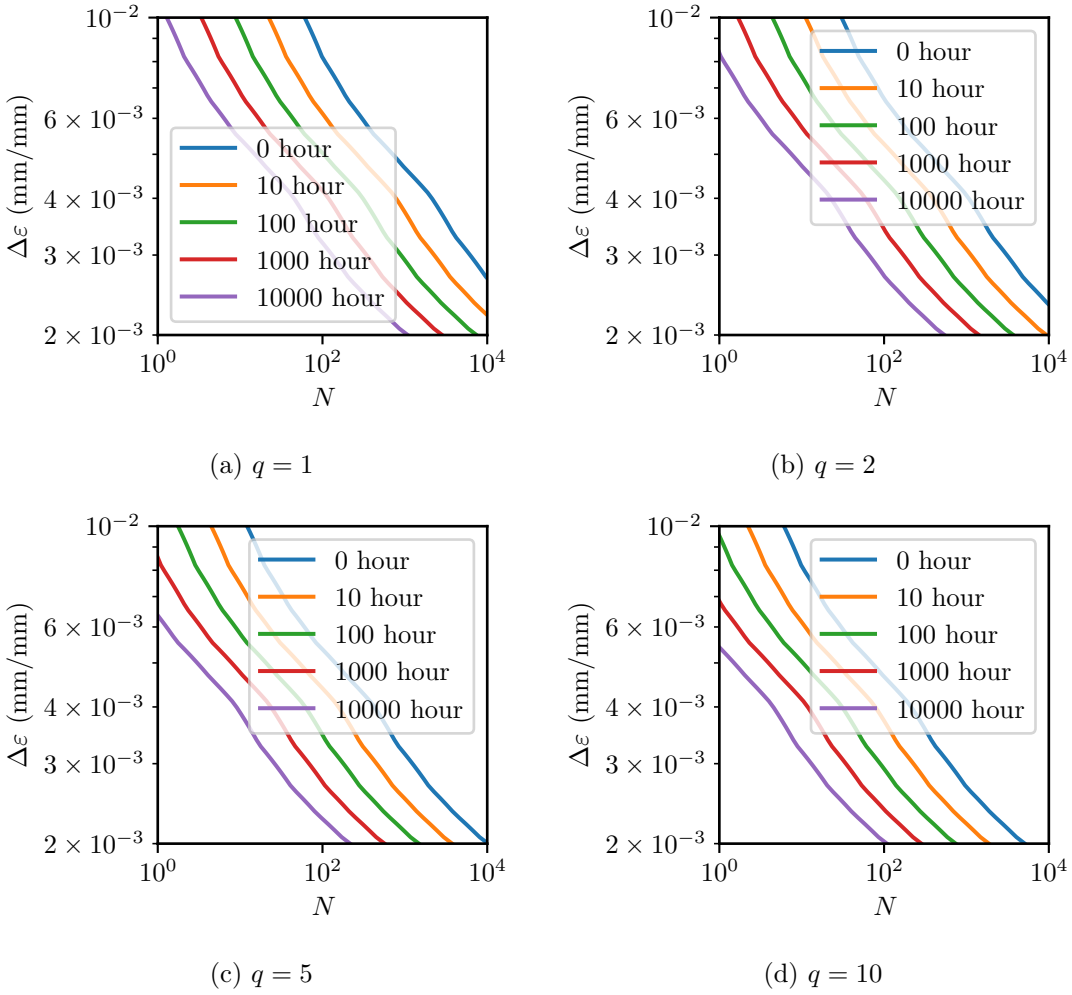

(a) $q = 1$

(b) $q = 2$

(c) $q = 5$

(d) $q = 10$

Figure 4.3: Prospective design curves for Grade 91 using the standard Coffin shift at 538° C.

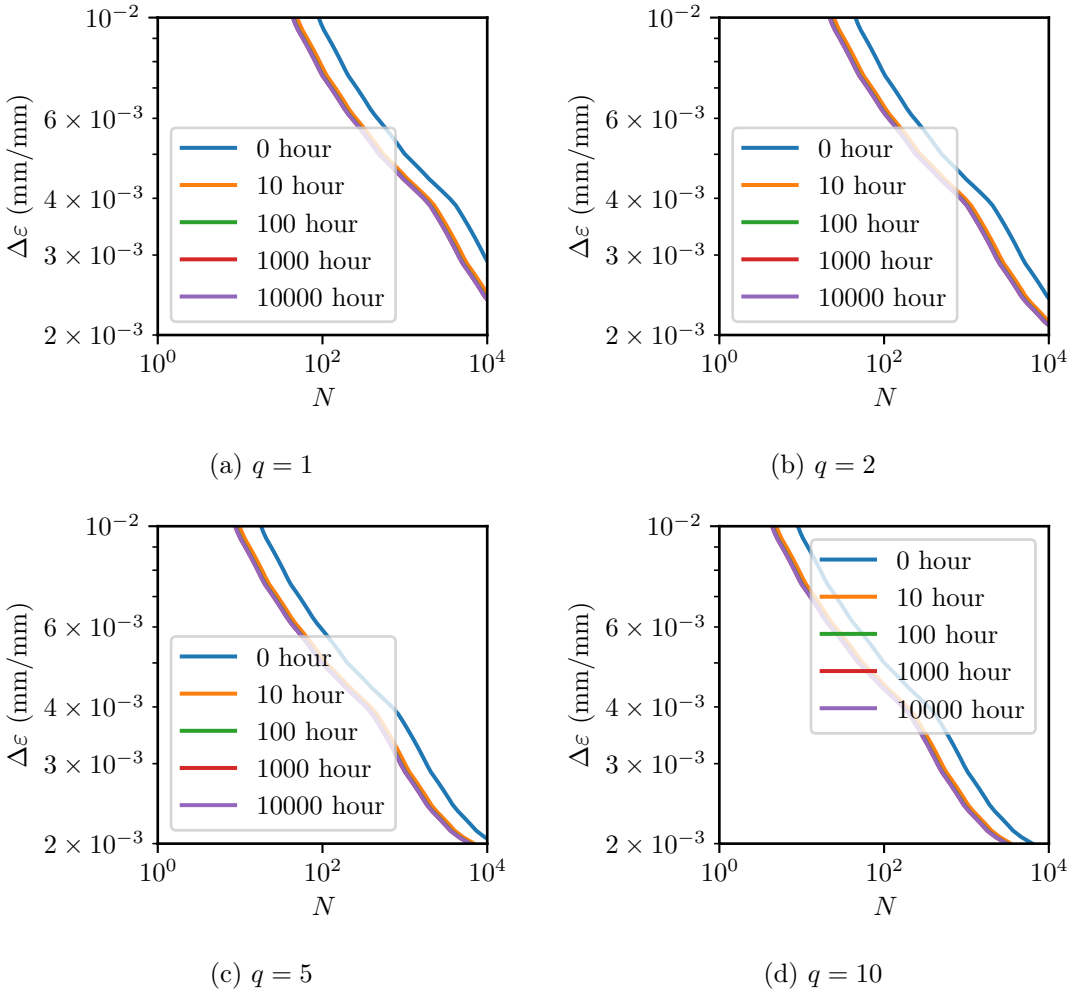

(a) $q = 1$

(b) $q = 2$

(c) $q = 5$

(d) $q = 10$

Figure 4.4: Prospective design curves for Grade 91 using the modified Coffin shift at 538° C.

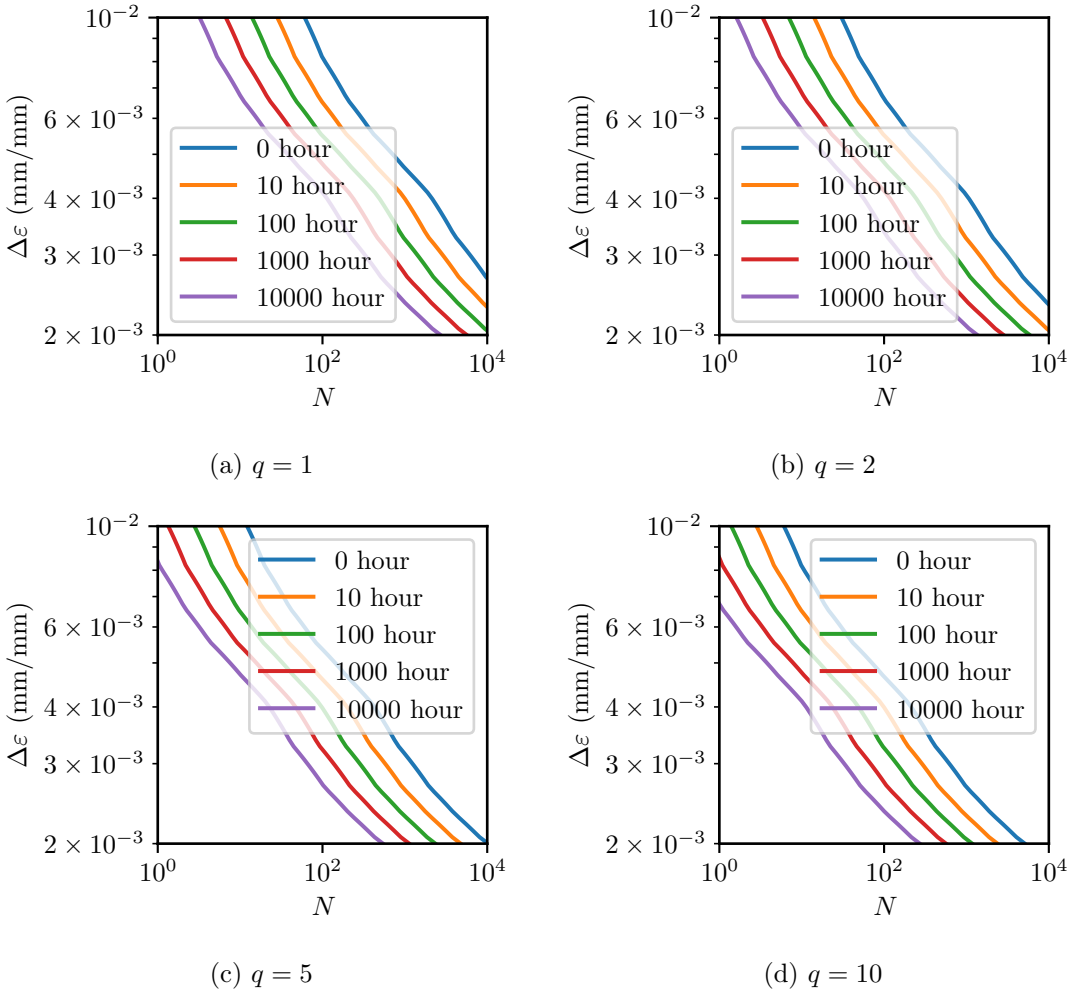

(a) $q = 1$

(b) $q = 2$

(c) $q = 5$

(d) $q = 10$

Figure 4.5: Prospective design curves for Grade 91 using the standard Coffin shift at 593° C.

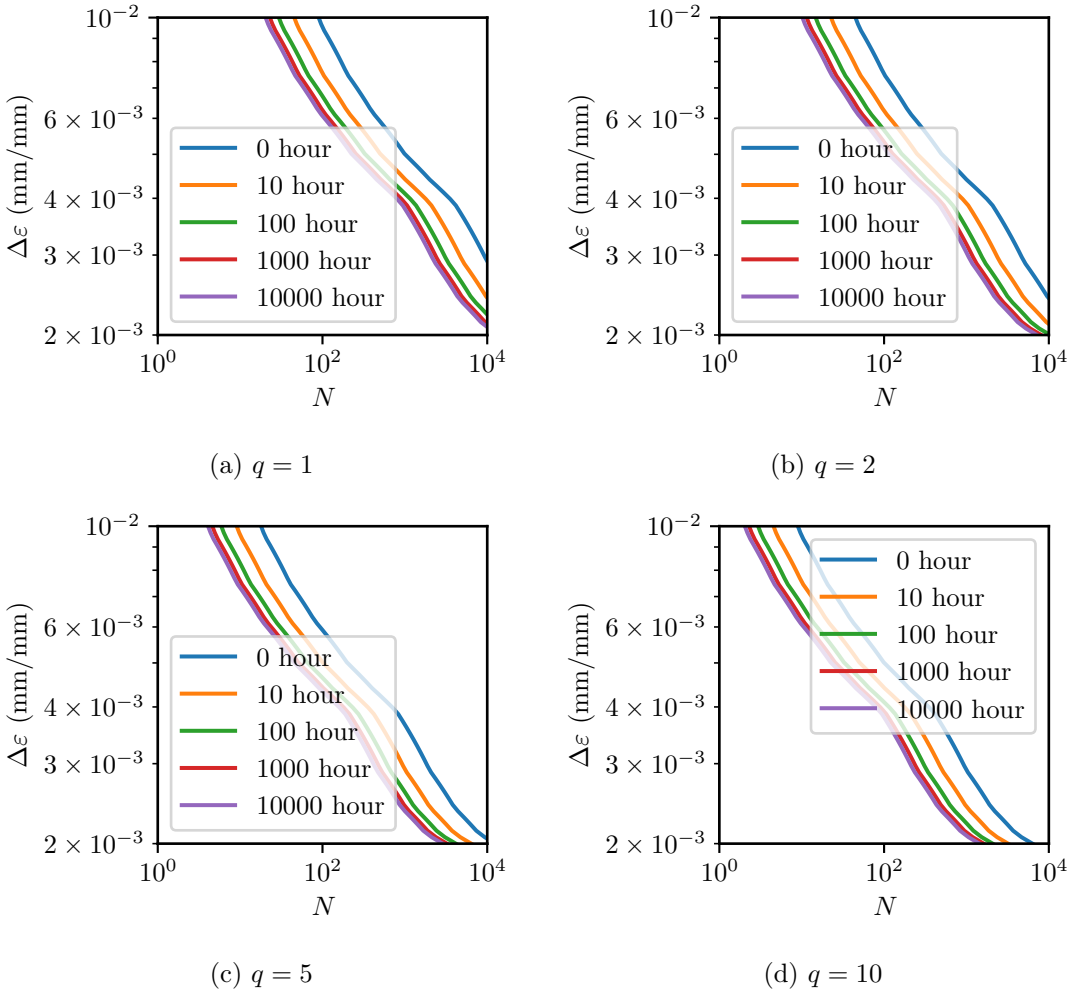

(a) $q = 1$

(b) $q = 2$

(c) $q = 5$

(d) $q = 10$

Figure 4.6: Prospective design curves for Grade 91 using the modified Coffin shift at 593° C.

From the design specification determine the number of design cycles for this loading cycle, N.

3. Develop a finite element model of the component subject to the cyclic loads identified in Step 1. This model must include local stress concentrations, including notches, holes, and other structural discontinuities. Because the analysis will use an elastic perfectly-plastic material model the applied boundary conditions may truncate any holds at constant load.

4. Define a temperature-dependent pseudoyield stress S_ε where S_ε is the stress value of the isochronous stress-strain curve for a 0.2% offset in strain from the elastic slope at a given temperature and for time t_h.

5. Run the finite element analysis using an elastic perfectly-plastic material model, using the Section II value of temperature dependent Young's modulus, the Section II Poisson's ratio, and the pseudoyield stress S_ε. Run multiple repetitions of the cyclic loading until the strain range over the cycle $\Delta\varepsilon$ becomes constant for all points in the structure[1]. This condition is guaranteed to occur [18].

6. For each point in the structure determine the maximum metal temperature occurring over the cycle. Enter the EPP+SMT design chart for this temperature at a strain range of $\Delta\varepsilon$ and hold time t_h to determine the allowable number of cycles N_a. The structure passes the creep-fatigue criteria if $N_a \geq N$ for all points in the component.

A companion report establishes life-fraction criteria for combining damage from load cycles of different types.

4.3 Comparison to current ASME methods

This trial design procedure can only be applied to uniaxial stress states. The simplest problem to consider is the elastic follow up two bar system shown in Fig. 2.1. Recall that for a elastic power law creep response in the gauge bar, the theoretical follow up factor of this system is

$$q = 1 + \frac{E_1}{E_2}. \tag{4.1}$$

The sample design problem considers fixing the total strain range applied to the two bar system and the follow up on the gauge bar, using Eq. 4.1, and calculating the creep-fatigue life of the gauge bar using five methods:

1. Section III, Division 5, Subsection HB, Subpart B Nonmandatory Appendix-T design by elastic analysis;

2. Section III, Division 5, Subsection HB, Subpart B Nonmandatory Appendix-T design by inelastic analysis using the material model defined in [19];

[1]For this report $\Delta\varepsilon$ corresponds to the axial strain in the direction of loading. The companion report defines an appropriate strain for multiaxial loading.

Parameter	Values	Units
$\Delta\varepsilon$	0.12,0.15,0.18	%
q	1,2,5,10	-
t_h	100	hours
T	528°	C

Table 4.1: Parameters used in the sample design problem.

3. Creep-fatigue design using elastic perfectly-plastic analysis with ASME Code Case N-862;

4. The design method defined here using the Coffin-shift design curves (Fig. 4.5);

5. The design method defined here using the modified Coffin-shift design curves (4.6).

Rather than choose a bounding value of follow up, for #4 and #5 this example uses the design chart corresponding to the actual follow up in the system calculated with Eq. 4.1. As described above, in the final design method a bounding value of q will be used instead. This alteration is advantageous for the new method proposed here, as it removes a conservative design approximation for low values of follow up. However, it allows this example to assess the differences between the design methods for low and high values of elastic follow up.

Table 4.1 lists the parameters used in the sample design problems and Fig. 2.1 shows the geometry. Note the definition of the imposed strain range applies to the gauge bar, not the total system. For this problem the length and cross-sectional areas of the bars does not affect the results. The results of the design checks are presented as the maximum allowable number of cycles allowed for the defined loading, using the particular design method. This requires iterative calculations as all five methods are setup as pass/fail checks.

In terms of design margin, the comparison between the ASME methods and the new method proposed here is not exactly fair. The new method starts with the factored fatigue design chart from Section III, Division 5, as with the three ASME methods. However, the ASME approaches also increases the stress relaxation history used to compute creep damage. There is no corresponding creep damage calculation in the new method. Future work will be required to determine if additional design factors are required for the EPP+SMT method to cover this additional margin in the ASME Code.

Table 4.2 lists the cyclic creep-fatigue life calculated for the two bar systems for several combinations of stress range and follow up factor. This table only accounts for the creep-fatigue design check, not counting any preliminary required checks. For example, for the ASME Section III, Division 5 methods the system must first pass the primary load check and the ratcheting check before creep-fatigue damage can be calculated. These preliminary checks are not performed for these results.

These combinations of strain ranges and hold times were selected to achieve non-zero cyclic lives when using the design by elastic analysis methods. For these very small strain ranges the SMT approach predicts orders of magnitude additional cyclic life compared to the current methods. These large predicted lives result from the constant shifted fatigue curves used to formulate the design method. For small strains, near the fatigue limit, a horizontal shift results in a negligible hold time effect (see Fig. 4.7). There is no experimental data

		q			
$\Delta\varepsilon$	Method	1.0	2.0	5.0	10.0
0.12%	E	299	299	299	299
	EPP	8472	8472	8472	8472
	I	9077	7516	5613	4497
	SMT-C	541864	270932	108372	54186
	SMT-M	32887487	16443743	6577497	3288748
0.15%	E	26	26	26	26
	EPP	4157	4157	4157	4157
	I	8165	6010	2998	1002
	SMT-C	98442	49221	19688	9844
	SMT-M	1105840	552920	221168	110584
0.18%	E	6	6	6	6
	EPP	650	650	650	650
	I	7074	4572	928	218
	SMT-C	24509	12254	4901	2450
	SMT-M	54869	27434	10973	5487

Table 4.2: Results from the comparative analysis of the two bar system accounting for the creep-fatigue design checks only. Hold time is 100 hours. Methodologies are design by *E*lastic analysis, design by *E*lastic *P*erfectly-*P*lastic analysis, design by *I*nelastic analysis, design with the new *SMT* method using the *C*offin shift, and design using the *SMT* method using the *M*odified Coffin shift.

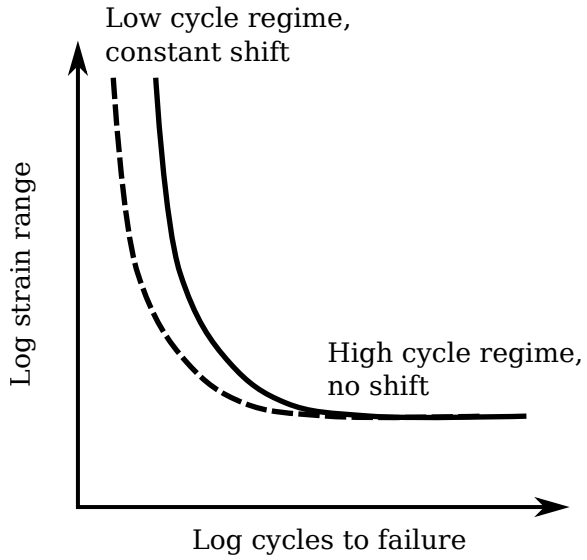

Figure 4.7: Schematic illustrating the effect of a constant shift on a log scale to a fatigue curve in the low cycle and high cycle regimes. As the material approaches the fatigue limit a shift has no effect on the design curve.

available to test the SMT method predictions in this regime because small strain range/long hold time tests would take a very long time to fail.

Table 4.3 presents an alternate comparison between design by inelastic analysis and the SMT methods for higher strain ranges and without factoring the stress relaxation history used to calculate creep damage in the design by inelastic analysis calculations. The base Code procedure divides the stress history from the analysis by a factor of 0.67 when calculating creep damage, here this factor is neglected. This approach fairly compares the design methods – both use factored fatigue curves and both do not factor on creep damage. These results show that the two methods are comparable – a factor of two to five on cyclic life is easily within experimental scatter – though the inelastic analysis method penalizes loads with significant follow up more than the EPP+SMT approaches.

Finally, Table 4.4 compares the inelastic and SMT design methods for a fixed strain range of $\Delta\varepsilon = 0.25\%$ and increasing hold times. Again, the design by inelastic analysis calculations do not include the 0.67 factor on the stress relaxation history.

These comparisons show that in low cycle fatigue range the SMT methods are both reasonable when compared to unfactored design by inelastic analysis. Generally, the SMT methods produce higher cyclic lives than inelastic analysis. All three design methods produce comparable values, given the experimental scatter in creep-fatigue data. Given the results of this comparison and the expectation of a saturating reduction in creep-fatigue life with increasing hold time, we recommend basing the SMT design method on the modified, saturating Coffin shift. This model fits the available experimental data and does not produce incompatible results, when compared to the current design by inelastic analysis method.

		q			
$\Delta\varepsilon$	Method	1.0	2.0	5.0	10.0
0.20%	I	2717	2591	2293	1889
	SMT-C	3215	1607	643	321
	SMT-M	5728	2864	1145	572
0.25%	I	1290	1185	802	459
	SMT-C	1424	712	284	172
	SMT-M	3004	1502	601	300
0.30%	I	467	185	33	0
	SMT-C	773	386	154	77
	SMT-M	1901	951	380	190

Table 4.3: Comparison between inelastic analysis and the SMT methods for larger strain ranges at a hold time of 100 hours. Methodologies are design by *I*nelastic analysis, design with the new *SMT* method using the *C*offin shift, and design using the *SMT* method using the *M*odified Coffin shift.

		q			
t_h (hrs)	Method	1.0	2.0	5.0	10.0
1	I	5382	3428	3320	3052
	SMT-C	14008	7004	2801	1401
	SMT-M	17420	8710	3484	1741
10	I	3343	3305	3171	2672
	SMT-C	6521	3260	1304	652
	SMT-M	8813	4406	1763	881
100	I	2717	2591	2293	1889
	SMT-C	3215	1608	643	321
	SMT-M	5729	2864	1146	573
1000	I	1034	922	750	634
	SMT-C	1547	774	309	155
	SMT-M	4455	2228	891	446
10000	I	136	121	107	95
	SMT-C	742	371	148	74
	SMT-M	3956	1978	791	396

Table 4.4: Comparison between inelastic analysis and the SMT methods for increasing hold times at a fixed strain range of 0.25%. Methodologies are design by *I*nelastic analysis, design with the new *SMT* method using the *C*offin shift, and design using the *SMT* method using the *M*odified Coffin shift.

A bounding value of q should be selected bases on results of analytical studies assessing elastic follow up in realistic high temperature components. However, the results here give insight into the practical effects of selecting a certain value of follow up. A bounding follow up factor in between $q = 2$ and $q = 5$ would scale the modified Coffin shift SMT method to produce comparable cyclic lives to unfactored design by inelastic analysis. A even higher value of q, say $q = 10$, may reasonably account for the creep damage design factor of 0.67 for inelastic analysis and 0.9 for elastic analysis when comparing the ASME methods to the new design methods. Even a bounding value of $q = 10$ does not shift the SMT results to differ widely from the unfactored inelastic results.

5 Conclusions

The central problem in completing the design method is determining which of the two behaviors illustrated on Figure 5.1 should be used when extrapolating creep effects into the high cycle fatigue range. Option A extrapolates the results of creep-fatigue and SMT tests at higher strain ranges. Option B determines an appropriate shift from the creep-fatigue and SMT data and then applies that uniform shift to the experimentally-determined fatigue curve. Both options are reasonable and direct testing to determine which is correct is impossible – high cycle fatigue tests with holds would take years to complete. Physically, we should expect some equivalent of the fatigue limit in plotted creep-fatigue data as low strain ranges will produce low stresses and negligible creep damage. However, again, it will be difficult to directly test this prediction for reasonable hold times. At the present we recommend the shifted fatigue curve option, as it produces the most reasonable results from the currently available data. A few long term creep-fatigue tests should be completed to validate this choice of extrapolation.

Developing finalized EPP+SMT design curves for the Class A materials will require:

1. Assembling the existing creep-fatigue data for each material, done for Alloy 617 is in this report. Additional testing should not be required for any of the current Class A materials, but this may require extensive library research to find the 304H and 2.25Cr-1Mo data. For Grade 91, 316H, and 800H the creep-fatigue test data is readily available.

2. Make a final decision on the choice of time extrapolation. This report recommends a modified Coffin approach for Alloy 617. Data for the other materials should be checked to ensure this recommendation does not need to be reexamined.

3. Make a final decision on the method of extrapolation – best fit to high strain range data or shifted fatigue curves. This report recommends the latter approach. Specialized, long-term creep-fatigue tests should be performed for a few materials to validate the approach.

4. Select a bounding follow up factor, any explicit design margin, and a method for capturing statistical scatter in the (sparse) data. This report suggests using a follow up factor of 10, no explicit additional factors, and mean-property shifts applied to the factored ASME fatigue curves.

5. Construct the design charts for each of the Class A materials, using the creep-fatigue data assembled in #1 and the methodology selected in #2 and #3.

6. Validate the extrapolations selected for hold time and follow up factor with single bar SMT tests.

This report, combined with the companion report on combining load cycles, describes a complete design method. This design method should be validated. Two options are available:

1. Validation by comparison to other design methods. The new EPP+SMT method should not produce results that are greatly inconsistent with other design methods, including the current methods in Section III, Division 5 of the ASME Code. This

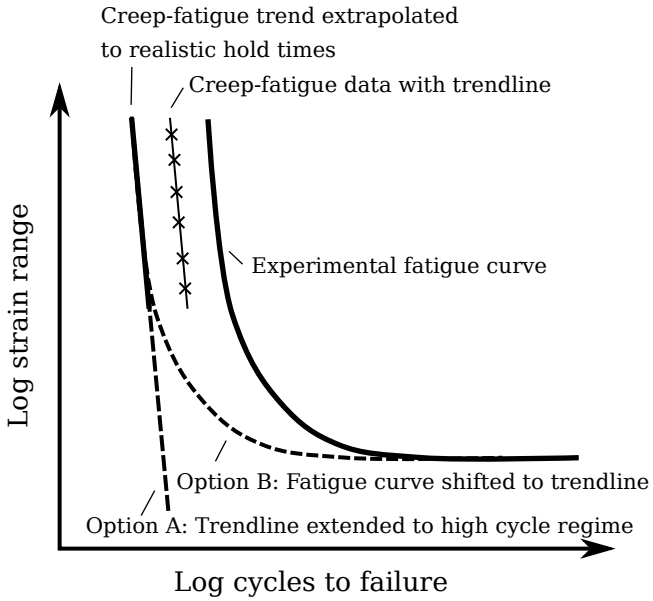

Figure 5.1: Sketch demonstrating two reasonable approaches to extrapolating the available high strain range, short hold time experimental data into the low strain range, long hold regime needed for engineering design.

type of validation is relatively easy to perform and can look at arbitrary component configurations and load histories. However, the results described in Chapter 4 above show that there will be differences from the current design methods when approaching the high cycle fatigue regime. It is not obvious that the current methods are correctly predicting life in this regime, so a decision will need to be made on whether to artificially alter the EPP+SMT method to conform with the current Division 5 approach or to accept the different predictions of cyclic life.

2. Validation by comparison to scaled component tests. This is the "gold standard" in that it directly assess the accuracy of the method against a realistic component geometry and loaded tested to failure. However, there are very few tests available from past DOE sponsored work and future testing will be limited by the cost and time required to conduct such scaled component testing.

A Alloy 617 test database

The following table lists records for 93 fatigue, creep-fatigue, and SMT tests on Alloy 617 samples at 950° C. This table combines the creep-fatigue results reported in the Alloy 617 ASME Code Case with SMT test data collected at ORNL [7, 15, 6, 4, 5]. The strain ranges are the controlled strain range for the fatigue and creep-fatigue tests ($q = 1$) and the EPP strain ranges for the SMT tests ($q > 1$). Hold directions are given in the table with codes indicating a tensile hold (T), compressive hold (C), both (T/C), or no hold (N).

$\Delta\varepsilon$ (%)	q	t_h (min)	Hold	N
0.3	1	0	N	9641
0.3	1	0	N	5867
0.3	1	0	N	9054
0.3	1	0	N	7133
0.3	1	0	N	8333
0.3	1	0.033	T	4083
0.3	1	0.033	T	3538
0.3	1	3	T	4486
0.3	1	3	T	3984
0.3	1	3	T	2485
0.3	1	10	T	4096
0.3	1	10	T	4430
0.3	1	10	T	2623
0.3	1	10	T	4361
0.3	1	30	T	4832
0.3	1	30	T	4650
0.3	1	30	T	2653
0.3	1	3	C	4373
0.3	1	3	T&C	1310
0.3	1	12	T&C	1159
0.4	1	0	N	2378
0.4	1	1	T	1680
0.4	1	0	N	2326
0.4	1	1	T	1768
0.6	1	0	N	1722
0.6	1	0	N	1390
0.6	1	0	N	1480
0.6	1	0	N	1342
0.6	1	0	N	1295
0.6	1	0	N	1432
0.6	1	0	N	1266
0.6	1	0	N	1085
0.6	1	1	T	1085
0.6	1	1	T	953
0.6	1	1	T	975
0.6	1	1	T	904

$\Delta\varepsilon$ (%)	q	t_h (min)	Hold	N
0.6	1	1	T	1048
0.6	1	3	T	950
0.6	1	3	T	922
0.6	1	10	T	686
0.6	1	10	T	634
0.6	1	10	T	547
0.6	1	30	T	661
0.6	1	30	T	1110
0.6	1	30	T	525
0.6	1	0	N	1498
0.6	1	0	N	1254
0.6	1	0	N	1233
0.6	1	0	N	1229
0.6	1	0	N	1506
0.6	1	1	T	826
0.6	1	1	T	986
0.6	1	1	T	1046
0.6	1	1	T	1054
0.6	1	1	T	937
1	1	0	N	963
1	1	0	N	972
1	1	0	N	916
1	1	0	N	897
1	1	0.033	T	820
1	1	0.033	T	790
1	1	3	T	376
1	1	3	T	465
1	1	3	T	472
1	1	10	T	308
1	1	10	T	391
1	1	10	T	427
1	1	10	T	430
1	1	30	T	322
1	1	30	T	364
1	1	30	T	334
1	1	150	T	386
0.206126	2.7	10	T	270
0.206126	2.7	10	T	940
0.206126	2.7	10	T	950
0.368072	2.7	10	T	370
0.368072	2.7	10	T	350
0.368072	2.7	10	C	1000
0.379492	2.7	20	T&C	400
0.063094	3.5	3	T	10660

$\Delta\varepsilon$ (%)	q	t_h (min)	Hold	N
0.254669	3.5	10	T	1000
0.254669	3.5	10	T	900
0.254669	3.5	10	T	1100
0.254669	3.5	10	C	1200
0.272193	3.5	20	T&C	1050
0.32547	3.5	0	N	1600
0.480447	3.5	10	T	460
0.480447	3.5	10	T	450
0.480447	3.5	10	T	950
0.480447	3.5	10	C	600
0.49797	3.5	20	T&C	600
0.507171	3.5	30	T	230
0.558454	3.5	600	T	150

Acknowledgments

The research was sponsored by the U.S. Department of Energy, under Contract No. DEAC02-06CH11357 with Argonne National Laboratory, managed and operated by UChicago Argonne LLC. Programmatic direction was provided by the Office of Nuclear Reactor Deployment of the Office of Nuclear Energy (NE).

The authors gratefully acknowledge the support provided by Diana Li of DOE-NE, Federal Manager, Advanced Reactor Technologies (ART) Program, Gas-Cooled Reactors (GCR) Campaign; Sue Lesica of DOE-NE, Federal Manager, ART Advanced Materials; and Gerhard Strydom of Idaho National Laboratory, National Technical Director, ART GCR Campaign.

Bibliography

[1] American Society of Mechanical Engineers, "Section III, Division 5," in *ASME Boiler and Pressure Vessel Code*, 2017.

[2] American Society of Mechanical Engineers, "Case N-862: Calculation of Creep-Fatigue for Division 5 Class A Components at Elevated Temperature Service Using Elastic-Perfectly Plastic Analysis," in *ASME Boiler and Pressure Vessel Code, Nuclear Component Code Cases*, 2015.

[3] Y. Wang, M. C. Messner, and T.-L. Sham, "Report on the FY18 Uniaxial Material Model Testing and Key Feature Test Articles Testing of Grade 91," tech. rep., Oak Ridge National Laboratory ORNL/TM-2018/885, 2018.

[4] Y. Wang, R. I. Jetter, M. C. Messner, and T.-L. Sham, "Report on FY18 Testing Results in Support of Integrated EPP-SMT Design Methods Development," tech. rep., Oak Ridge National Laboratory ORNL/TM-2018/887, 2018.

[5] Y. Wang, R. I. Jetter, and T.-L. Sham, "Report on FY17 Testing in Support of Integrated EPP-SMT Design Methods Development," tech. rep., Oak Ridge National Laboratory ORNL/TM-2017/351, 2017.

[6] Y. Wang, R. I. Jetter, and T.-L. Sham, "FY16 Progress Report on Test Results In Support Of Integrated EPP and SMT Design Methods Development," tech. rep., 2016.

[7] Y. Wang, R. I. Jetter, K. Krishnan, and T.-L. Sham, "Progress Report on Creep-Fatigue Design Method Development Based on SMT Approach for Alloy 617," tech. rep., Oak Ridge National Laboratory ORNL/TM-2013/349, 2013.

[8] R. I. Jetter, "An Alternate Approach to Evaluation of Creep-Fatigue Damage for High Temperature Structural Design Criteria," in *Fatigue, Fracture and High Temperature Design Methods in Pressure Vessel and Piping*, American Society of Mechanical Engineers Press, 1998.

[9] M. C. Messner, T.-L. Sham, Y. Wang, and R. I. Jetter, "Evaluation of methods to determine strain ranges for use in SMT design curves," tech. rep., Argonne National Laboratory ANL-ART-138, 2018.

[10] R. Hales, S. R. Holdsworth, M. P. O'Donnell, I. J. Perrin, and R. P. Skelton, "A Code of Practice for the determination of cyclic stress-strain data," *Materials at High Temperatures*, vol. 19, no. 4, pp. 165–185, 2014.

[11] J. Lemaitre and J. L. Chaboche, *Mechanics of Solid Materials*. Cambridge University Press, 1994.

[12] R. M. Goldhoff, "Uniaxial Creep-Rupture Behavior of Low-Alloy Steel Under Variable Loading Conditions," *Journal of Basic Engineering*, vol. 87, no. 2, pp. 374–378, 1965.

[13] W. Ostergren, "Correlation of hold time effects in elevated temperature low cycle fatigue using a frequency modified damage function," in *Proceedings of the ASME-MPC Symposium on Creep/Fatigue Interaction*, 1976.

[14] J. Lemaitre, "How to use damage mechanics," *Nuclear Engineering and Design*, vol. 80, pp. 233–245, 1984.

[15] Y. Wang, R. I. Jetter, S. T. Baird, C. Pu, and T.-L. Sham, "Report on FY15 Alloy 617 SMT Creep- Fatigue Test Results," tech. rep., Oak Ridge National Laboratory ORNL/TM-2015/30, 2015.

[16] L. F. Coffin, "The concept of frequency separation in life prediction for time," in *Proceedings of the ASME-MPC Symposium on Creep/Fatigue Interaction*, 1976.

[17] T. Asayama and Y. Tachibana, *Existing Evaluation Procedures for Grade 91 and Hastelloy XR.* 2009.

[18] C. O. Frederick and P. J. Armstrong, "Convergent internal stresses and steady cyclic states of stress," *The Journal of Strain Analysis for Engineering Design*, vol. 1, no. 2, pp. 154–159, 1966.

[19] M. C. Messner, V.-T. Phan, and T.-L. Sham, "A Unified Inelastic Constitutive Model for the Average Engineering Response of Grade 91 Steel," in *Proceedings of the 2018 ASME Pressure Vessels and Piping Conference*, PVP2018-84104, 2018.

Applied Materials Division
Argonne National Laboratory
9700 South Cass Avenue, Bldg. 212
Argonne, IL 60439

www.anl.gov